DISTRIBUTED AUTONOMOUS CONTROL ACTION BASED ON SENSOR AND MISSION FUSION

June 1, 2004 – August 31, 2005

FINAL REPORT

Submitted to the

OFFICE OF NAVAL RESEARCH

Principal Investigator: Stephen Konyk, Jr.
Research Associate: Ashish Swaminathan

Center for Advanced Communications
Villanova University
Villanova, PA 19085

September, 2005

ABSTRACT

The research effort focuses on the exploration of sensing and control techniques in the framework of fusion and distributed control pertinent to the problem of deploying autonomous unmanned surface platforms and clusters of platforms in mission applications in support of future naval capability. The considerations which comprise the approach to the distributed autonomous problem are threefold: (1) platform sensing capability for environment and mission; (2) distributed based control of autonomous platforms and clusters; (3) the intelligent fusion of sensor data, mission and control action. Fundamentally, the effort deals with the study of pertinent modeling approaches which may be useful in enhancing the processing and fusion of data to achieve appropriate distributed control action. This provides a vehicle for the exploration of mission specific distributed autonomous platform performance. From a real-time application perspective, the real-time turnaround, time correlation and the adaptability of a fusion based distributed control are of concern. This requires the development of novel approaches to sensor return integration and interpretation in conjunction with novel approaches to developing a fusion based distributed control strategy capable of adaptation, learning and information sharing. Potential mission applications include the implementation of these techniques in unmanned vehicle control, mine warfare, anti-submarine warfare, and anti-terrorism/force protection.

TABLE OF CONTENTS

1.0 INTRODUCTION

The envisioned US Navy future naval capability incorporates the development of autonomous unmanned platforms and cluster of platforms [5]. This autonomous platform architecture may comprise of thousands of fully netted unmanned vehicles and unattended sensors (e.g. FORCEnet) as illustrated in Figure 1. Key to the success of this concept is the ability to maintain a functional network of autonomous distributed platforms deployed as sensors and combatants.

1.1 Application Overview

Crucial to the successful realization of such a system is the development of the capability of maintaining real-time sensor data turnaround in concert with autonomous formation control driven by mission requirements and environmental assessment based on sensor fusion. Techniques applied to attain distributed autonomous platform cluster survivability and autonomous formation control are critical in accomplishing a hostile environment mission.

The effort presented addresses these critical issues in the context of seeking to develop innovative approaches for sensor data fusion and in the incorporation of the fused data for adaptive distributed autonomous control in formation control, addressing mission and operating environment. Pertinent naval applications include unmanned vehicle control (e.g. UV), mine and undersea warfare (MUW), anti-submarine warfare (ASW), and anti-terrorism/force protection (ATFP).
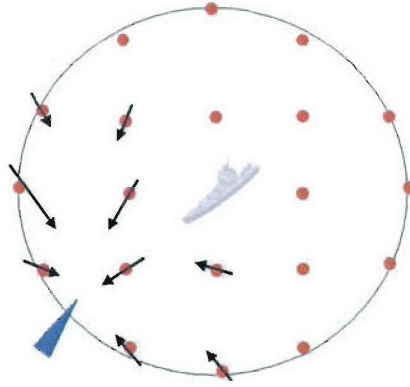
Figure 1: Illustration of large-scale autonomous operations.

1.2 Problem Description

The fundamental problem of investigating an approach to autonomous platform distributed formation control based on aspects of sensor fusion pertinent to platform-to-platform sensing is addressed. The research focuses on time delay aspects of sensing and on real-time autonomous intelligent navigational trajectory generation [19], [20]. The former is an issue when the separation between platforms is very large compared to the duration of signals generated in the operating environment. The latter deals with formation control of network of autonomous vehicles which are capable of adaptation based on the sensed operating environment, condition of the platform and mission objectives.

Section 2.0 of the report presents results on autonomous navigation and control. The formation control problem is investigated from the perspective of employing a vector integration to endpoint differential structure to adaptively generate trajectories while maintaining a coordinate map base of the fusion environment. The combination of sensing, formation control and mission fusion addresses current critical limitations in

implementing a full scale operational autonomous platform network. The modeling and simulation of these processes will provide a basis for performance assessment and future development.

Section 3.0 of the report presents results on the autonomous sensing problem for distributed agents with application to autonomous surface vehicle distributed fluid supply systems. The sensing problem concerns itself with the efficient estimation of the time-of-flight associated with acoustic signals between separated platform sensors. The use of hyper-geometric properties will be investigated as a means of reducing the number of sensors for identification of time-of-flight and as a means of reducing computational complexity in fusing the sensor-to-sensor data.

2.0 AUTONOMOUS NAVIGATION

This section describes a novel fusion and learning approach developed for autonomous navigation of UAV platforms. The approach consists of incorporating adaptation into a vector integration neural navigation model in conjunction with parametric fuzzy adaptation for mission fusion.

2.1 Autonomous Control Methodology

The vector-integration-to-endpoint model of the neural dynamics of planned arm movements consists of two coupled equations which may be directly applied to autonomous platform navigation and formation control. These equations form a model basis for sequentially updating the present platform coordinate position in real-time to attain a desired target coordinate for platform motion. These position updates are driven by a mismatch between the present coordinate position of the platform and the desired final coordinate target position. In its basic form, the VITE model is a real-time neural network which, for the ith entry of the coordinate vector, may be expressed as [17], [14]:

$$\frac{d}{dt}V_i = \alpha(-V_i + T_i - P_i) \tag{1}$$

$$\frac{d}{dt}P_{ii} = G[\max(V_i, 0)] \tag{2}$$

where T_i is the ith entry of the desired position coordinate vector T of the platform; P_i the ith coordinate of the present position command coordinate vector, P; V_i the ith coordinate of the mismatch vector, V; and G is a possibly time varying velocity command termed the "GO" signal.

The first equation generates a nonzero mismatch vector V whenever the present position command coordinate vector P differs from the desired position vector T. The mismatch vector is continually added to the present position command vector, P, until the present position command vector equals the desired position vector and a zero valued mismatch vector results.

The above trajectory generator permits multiple platforms to operate synchronously in time even though the coordinate distances from present position to final position may be different for each coordinate. Furthermore, the gain G, the "GO" signal, regulates the speed at which the path to the desired target position evolves. Even though G varies with time synchronous platform operation is maintained. Thus, the VITE model is capable of exhibiting many types of arm motion characteristics. These include the capacity to speed up, slow down and fast freeze anywhere along a trajectory path. This is accomplished by simply adjusting the GO signal gains in the model since the value of these gains determines the rate at which the trajectory evolves in real-time. Increasing the gains results in faster motion, decreasing them slows motion and setting them to zero causes trajectory evolution to freeze. Such a feature is attractive in an environment where obstacles may suddenly appear along a trajectory.

The gain G also provides a means of regulating the update rate of the present position vector, P, by employing feedback from position sensors in the platform. The

gain G is adjusted to maintain a desired tracking error. If the actual tracking error exceeds that desired, the gain G may be reduced thereby sacrificing speed and improving accuracy. On the other hand, if the tracking error is less than that desired, the gain G may be made larger to increase speed while sacrificing accuracy.

In order to assure satisfactory UAV navigation path tracking accuracy, the discrepancy between trajectory generator present position commands and the actual position of the autonomous platform must be established and employed by the trajectory generator. A structure for an automatic learning process to accomplish this employs error signals derived from discrepancies between the autonomous platform actual position vector and that seen by the trajectory generator. This provides a means to adaptively tune the present position vector until it coincides with the actual position vector and the trajectory generator learns the actual position of the platform. This type of learning happens during periods of tracking inaccuracy, i.e. mismatch and allows the navigation updates to anticipate platform navigational dynamics. The learning and trajectory update functions may be characterized by:

$$\frac{d}{dt}P_i = G[\max(V_{i,}0)] + G_p[\max(M_i,0)] \tag{3}$$

$$\frac{d}{dt}M_i = -\beta M_i + \gamma_i I - z_i P_i \tag{4}$$

$$\frac{d}{dt}z_i = \delta G_P\{-\varepsilon z_i + \max(M_i,0)\} \tag{5}$$

Equation (3) has replaced (1) and the second term on the right represents a gate update signal which is turned on by the gain G_P. M_i is another mismatch term driven by any difference between the actual position, γ_i, and the present position command, P_i. The variable z_i is an associative weight which readjusts the trajectory generator present position until it coincides with the actual position. The gains G and G_P enable external intelligent control of the update and learning functions.

2.2 Sensor fusion model based on Navigation control methodology

In automating the operation of a UAV and cluster of UAV's, a fundamental objective is to emulate the action of a skilled human operator. The sensor complement, in effect, must allow the autonomous intelligent navigation controller to discern the condition of the UAV platform system and to a degree of resolution comparable to that of the human operator. This includes the estimation of location and magnitude of piping leakage failures, assessment of sensor functionality and failure contingency operation. This involves the fusion of sensor information subject to constraints imposed by the system. This may be viewed as a constrained estimation and identification problem which projects noisy sensor data onto a constraint surface representing the physical model of pressure wave propagation [13], [12], [16]. The intelligent controller assesses the action that must be taken to optimize system performance. This requires the integration of the sensor fusion process into the control structure. Two methods of accomplishing this integration process are fuzzy logic and neural networks. These integration approaches are now discussed.

2.3 Fuzzy Theoretic formulation of Automation

The process of fuzzy logic provides a means of establishing a projection from a domain space of system parameters to a range space of assessment and control variables. The set of system domain space parameters may be quite diverse including not only various physical variables (e.g. navigational pipes, temperatures, propagation speeds, and pressures) but may incorporate variables which indicate the urgency with which a desired command should be executed by the system. The space of all domain variables forms the universe of discourse for fuzzy inference. The domain space is projected or mapped into the range space by interpreting a set of rules. The rules are linguistic statements having an antecedent-consequent, i.e. if-then, format. The rules are derived from an intelligent understanding of the operation of a particular system and can reflect imprecision and uncertainty. The rule set is evaluated in parallel and the order of evaluation is not critical. The resulting evaluation of the rule base is a subset set of elements in the range space. In the present context, the range space elements represent condition and control variables which are to guide the system in executing a prescribed command in the "best way" possible subject to the current conditions [13], [23], [24].

Prior to implementing the fuzzy inference process for a particular system the variables of the domain and range space must be defined and a means of characterizing the values these variables can take on must be provided. In addition a structure for the rule base must be established. These items and concerns are addressed next in Section 2.3.1 through 2.3.7. In addition summary overheads are provided in APPENDIX B.

2.3.1 Fuzzy Sets

Fuzzy sets are the domain and range elements on which the rule base operates. Consider a classical set such as $A = \{x | 0 \leq x \leq 6\}$. The membership of this set is well defined and for any $x \in R$ either $x \in A$ or $x \notin A$. The notion of a fuzzy set stems from relaxing the sharp classification criterion. Membership in a fuzzy set is characterized by specifying an element along with a measure of how much the element belongs to the set. That is, the elements of a fuzzy set, F, have the ordered pair form $(x, m(x)) \in F$ where x a well-defined element as in the classical set case and $m(x)$ is the membership function associated with how strongly x fits into F. The values of a membership function are typically restricted to the range $0 \leq m(x) \leq 1.0$. Where $m(x) = 0$ indicates that x is least likely to fit into the fuzzy set while $m(x) = 1.0$ indicates that x most likely to be a member of the fuzzy set. This set structure allows two things to happen. Firstly all subsets of the domain space, which correspond to rule premises, have membership of an element x assessed by a mapping to a membership value between 0.0 and 1.0. Secondly these mapping values provide a means of projecting how strongly the premises of a rule are satisfied and hence how strongly the conclusion should be emphasized.

2.3.2 Fuzzy Logical Operations

The interrelationship between the elements and subsets in classical set theory are well defined by an algebraic structure terms of unions, intersections, complements and differences. These operations are closed, commutative, associative and distributive. The truth or validity of a logical statement may be determined from these operations and properties. An extension of this process has been developed for fuzzy set algebra. Let

9

$A = \{(x, m_A(x))\}$ and $B = \{(x, m_B(x))\}$ be fuzzy sets over the domain space. Then the union of these sets is given by $A \cap B = \{x, S(m_A(x), m_B(x)\}$. Where the properties of the function S are chosen to yield classical set theoretic relationships when the membership functions are reduce the binary values of 0 and 1. Thus classical sets are a subspace of fuzzy sets. The function S must be monotonic, commutative and associative. Two commonly employed functions which satisfy these properties are the minimum function relation given by $S \equiv \min(m_A(x), m_B(x))$ and the product function relation given by $S \equiv product(m_A(x), m_B(x))$. Further continuing in the same vein, the union of two fuzzy domain space sets is given by $A \cup B = \{x, S(m_A(x), m_B(x)\}$ where S again must satisfy the conditions stated above. Commonly employed functions which satisfy these conditions include the maximum relation given by $S \equiv \max(m_A(x), m_B(x))$ and also the relation $S \equiv m_A(x) + m_B(x) - m_A(x) \times m_B(x)$ which has been termed the probabilistic OR function.

2.3.3 Fuzzy Logic Process

In implementing a fuzzy inference system several processes must be accomplished to map the domain space variables to the output space. These processes consist of: (1) a fuzzification interface for the input variable; (2) applying fuzzy union and intersection operations; (3) applying a fuzzy inference mechanism; (4) defuzzification interface which maps the conclusions of the inference mechanism to generate an output with the objective of controlling and or assessing the system [30], [24], [21].The method in which these four steps or processes are implemented characterized in large part the response dynamics of the fuzzy deduction process. Further details about each of these steps are considered next.

2.3.4 Fuzzification

The process of fuzzification consists of assigning the degree to which each parameter in the domain space belongs to the fuzzy sets which comprise the premises for the deduction rule set. This determines which rules are to be used and the extent to which the rule will influence the final outcome of the fuzzy logic process. Fuzzification is accomplished by employing a membership function. The fundamental characteristics of a sigmoidal membership function are shown Figure 2. The range of the membership function is from 0.0 to 1.0. This range of values expresses the confidence with which domain space elements belong to a particular fuzzy set. The membership function value 1.0 represents certain membership while the membership function value 0.0 indicates lack of membership. The process of Fuzzification consists of resolving the input, i.e. the domain, variables into their degree of membership in each of the antecedent fuzzy sets. In the case where the fuzzy rule base contains rules with multiple part antecedents, fuzzy set operations must be applied to blend the antecedents into a single number between 0.0 and 1.0. This process typically involves the intersection (AND) and union (OR) operations on fuzzy set elements previously defined. In any case, the fuzzification process assigns a single number to the antecedent for each rule in the rule base. Then next step in the process is one of assessing the validity of the conclusions associated with the various rules.
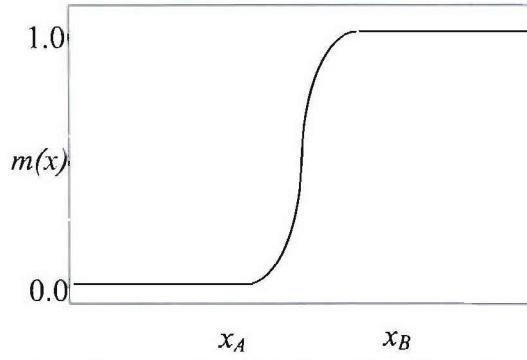
Figure 2: Illustration of a membership function for a domain space variable x.

2.3.5 Rule Implication Process

The process of implication determines what the conclusion of the fuzzy logic process will be. The previous fuzzification process determined which rules are active in the inference process. The recommendation of each rule is first considered individually. Each rule has associated with it a weight between 0.0 and 1.0 which is applied to the antecedent. This rule weight provides a means of tuning the relative influence of each rule on the outcome. These weighted individual recommendations are then blended into an aggregate conclusion which is the net recommendation of the fuzzy inference system in controlling the system or estimating its condition.

The outcome of each rule is a consequent that is a fuzzy set with an associated membership function that weighs the linguistic content of the rule. The input to the implication process is a single number derived from the antecedent and the resulting output is a fuzzy set. The implication process is done on a premise fuzzy set derived by an intersection, i.e. an AND, operation where the respective membership functions are derived from $S \equiv min$, i.e. minimum, operator or from $S \equiv prod$, i.e. product, operator. The former operation truncates the resultant fuzzy set while the latter operation scales the resultant fuzzy set.

2.3.6 Aggregation of the Rule Outputs

The fuzzy inference system in effect tests all of the rules in the rule base and then must combine all of the rule results in some fashion so as to derive a net decision or conclusion. The process of aggregation consists of combining the fuzzy sets that are the outputs of each rule in the rule base to form a single fuzzy set. The resulting single fuzzy set represents the final conclusion of the entire rule base. The aggregation method is typically a commutative process in which the order in which the rules are applied is unimportant. The fuzzy sets, which are the consequence of the rule base, may be combined commutatively with several common functions. The membership functions of the rule consequents may be combined using the maximum function, the probabilistic OR, and the sum function. The aggregation process employed in this work is the maximum function as described in the previous section. Application of this function commutatively combines all of the membership functions from the consequent of each rule into an aggregate membership function that describes the resulting final fuzzy set, i.e. the conclusion derived from the entire rule base.

2.3.7 Defuzzification to Generate Output

The structure of the controller considered requires that the output of the fuzzy logic process be a scalar quantity as opposed to a fuzzy set. Defuzzification is the conversion of a fuzzy set characterization of the outcome of the fuzzy logic process to a single scalar quantity. The output of a fuzzy logic process consists of the logical union of two or more fuzzy membership functions defined on the output variables. The center-of-gravity method is employed to defuzzify the output of the fuzzy logic process. This method is

perhaps the most well known and physically tractable approach to defuzzification, [24]. A scalar output, u_{net}, is obtained by operating on the membership function, $m_{net}(x)$, of the conclusion of the fuzzy logic process. The scalar output is given by the expression

$$u_{net} = \frac{\int \{m_{net}(x) \times x\} dx}{\int m_{net}(x) dx} \qquad (6)$$

where x represents the range of values which the fuzzy set output encompasses. Thus the center-of-gravity method calculates an average u_{net} of all possible output values x weighted by the degree of membership $m_{net}(x)$ of the output fuzzy set. This method is heuristic and generally performs well if the experience of system operators is integrated with analytical system models.

2.4 Neural network sensor fusion and autonomous control action

An architecture for UAV system intelligent autonomous control employing a neural network is shown in Figure 3. One of the most crucial considerations in formulating a neural based control process is the selection of neural network inputs and outputs [14], [15], [21], [30]. In the proposed neural controller, navigation position readings along with navigation generator states have been selected as inputs to the network. The network outputs are the various steering and thrust control signals. The neural network has the capability to learn dynamic control sequences and to interpolate intelligent control actions for system states which were not part of the original training algorithm.
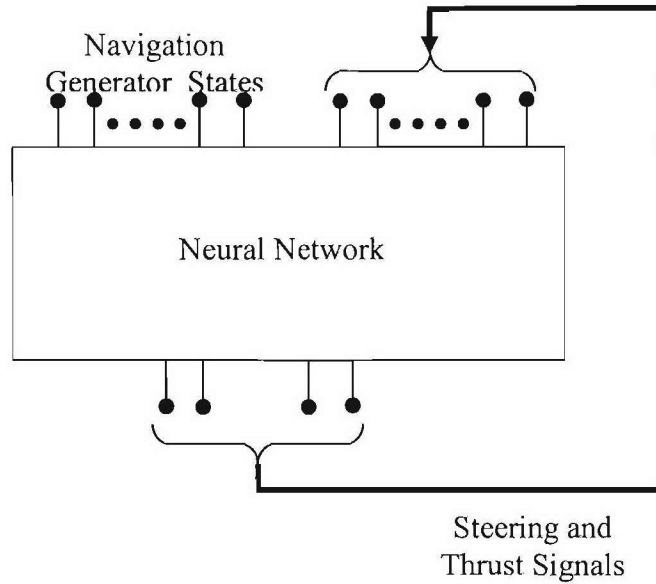
Figure 3: A neural network architecture for autonomous UAV system control.

Another crucial factor in the implementation of the neural network is the training sequence selected. The neural network can provide significant advantages in cases where the system model is not well defined and/or where a system inverse controller is employed. In these cases the network may be trained from data generated from actual system operation. In cases where the analytical model of the system is well defined, the neural network may provide a means of realizing various control actions which may be non-linear. In the context of the UAV system an autonomous intelligent control rule and action base must be established prior attempting a training algorithm formulation.

2.5 SIMULATION MODEL

The baseline considerations in using autonomous platforms are: navigational control of autonomous platforms and platform clusters; sensing capability for environment/mission; and the intelligent fusion of sensor, mission and control data. Key to the success of this

concept is the ability to maintain functionality while restricting navigational and sensor information bandwidths to acceptable levels. A vector integration to endpoint navigation model is employed as a distributed automata agent to satisfy the operational and information rate concerns. Simulation results illustrate the different characteristics of this model based on equations (1) and (2).

2.5.1 Autonomous Vehicle Challenges

The main challenges in implementing a navigational system include realizing the properties of:

1) Fast real-time capability:

   a) Maintain computational efficiency of the navigational model.

   b) Minimize communication bandwidth between different units.

2) Implicitly provide for the fusion of mission objectives and navigation goals. The goal of the above properties is the achievement of tracking accuracy as which seeks to minimize the difference between trajectory generator present position and the actual position of the autonomous platform. The rate of navigation progression must be adjusted based on the ability of the autonomous platform to follow trajectory commands. In effect, the navigation engine learns the UAV response characteristics and adjusts navigation commands to accommodate them.

2.5.2 Obstacle Avoidance Rule Set

One of the primary navigational functions which must be accomplished is that of obstacle avoidance. The navigation model must steer the vehicle to clear any obstacles with

respect to an x, y coordinate system, the baseline rule set chosen for collision avoidance is as follows:

- If Δx is large then make no correction.

- If Δy is large then make no correction.

- If Δx is small and Δy is small then take corrective action.

- If Δx is small and Δy is smallest then take corrective action emphasizing y.

- If Δx is smallest and Δy is small then take corrective action emphasizing x.

2.5.3 Navigation Model Simulation Performance

The performance of the integration to endpoint based navigation model is presented for the cases of open sea navigation with: (1) no hazards; (2) with hazards; (3) with moving hazards and (4) finally intercept of moving targets without and with stand off.

2.5.3.1 Open Sea Navigation Without Obstacle

Figure 4 shows the simulated path motion of the vehicle with no obstacle present in its path. The vehicle starts from coordinates (2,2) with its final target position being (10,10). The navigation motion is inherently smooth in position and velocity. Also, the changes in x and y coordinates are synergetic from start to stop. The generator exhibits non-oscillatory convergence throughout the open sea field of navigation.
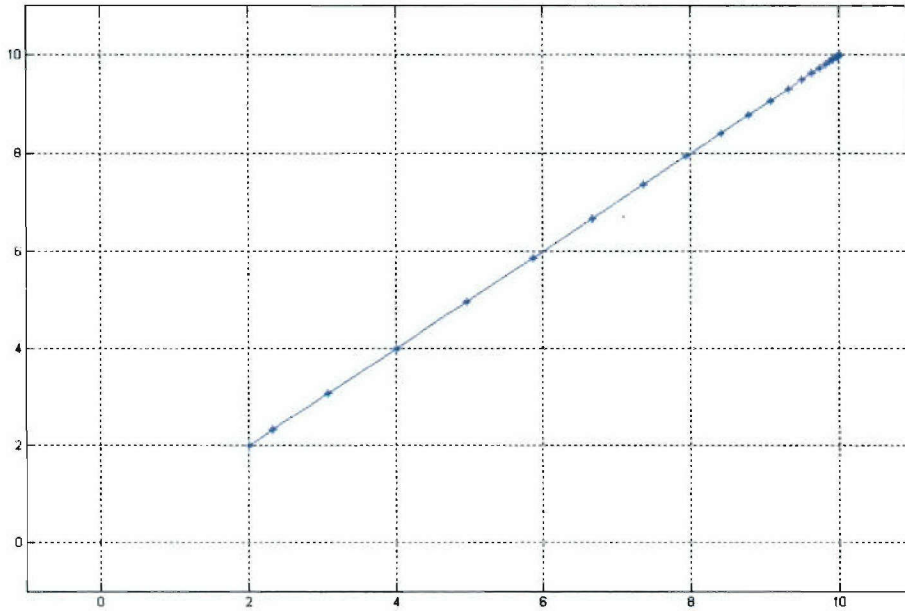
Figure 4: Navigation path without obstacles

2.5.3.2 Open Sea Navigation With Hazards

Figures 5 and 6 illustrate typical simulation results for the motion of a vehicle around circular hazards of differing diameters. The vehicle autonomously changes its path as it nears obstacles. It is observed that the coordinate points become more dense near the final position indicating smooth slowing velocity as the coordinates are approached. The navigation trajectories generated continue to exhibit non-oscillatory monotonic convergence which is smooth in position and velocity throughout the navigation region. A functional characterization of the obstacle avoidance navigation engine is presented in Figure 7.
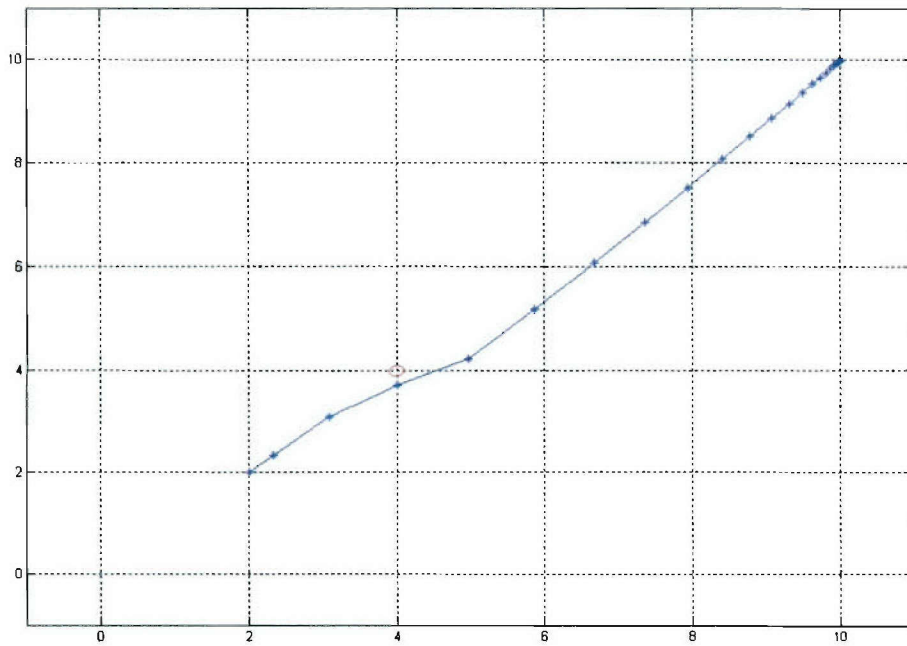
Figure 5: Navigation path with obstacle at (4,4)
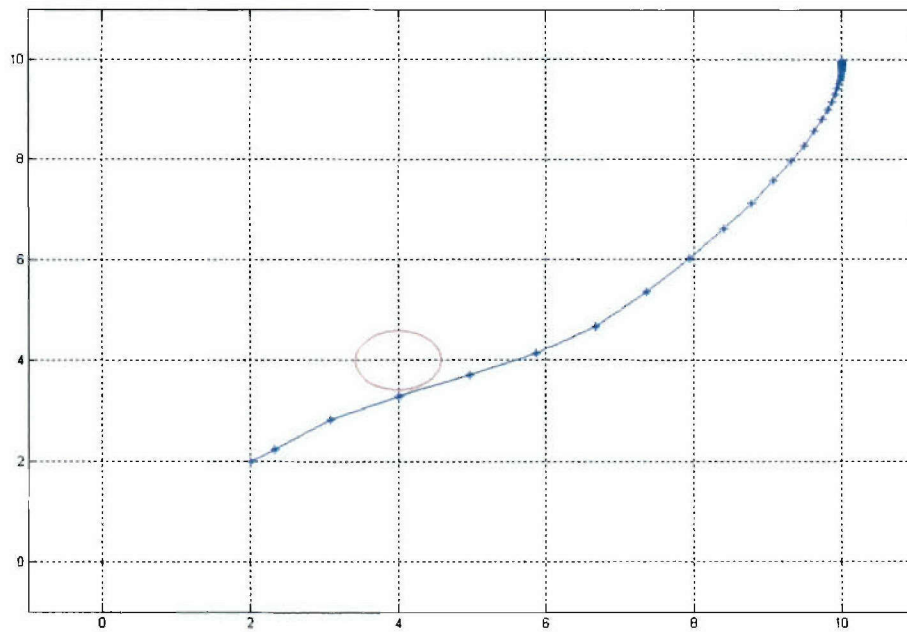
Figure 6: Navigation path with obstacle of diameter 1.16 at (4,4)

19
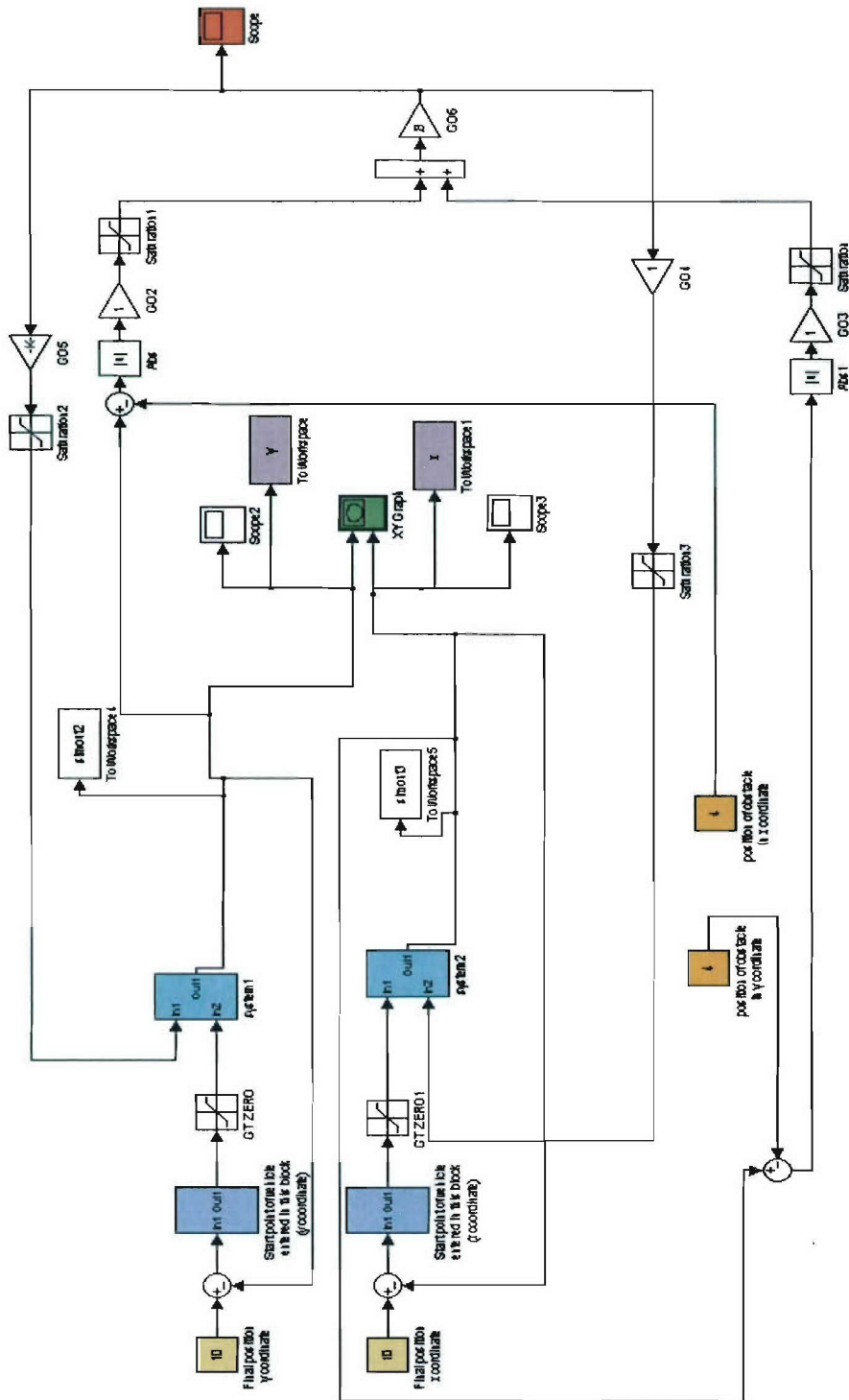
Figure 7: Functional characterization of obstacle avoidance

2.5.3.3 Open Sea Navigation with Moving and Fixed Hazards

Figures 8 and 9 show two vehicles on a collision course. In this case the obstacle avoidance algorithm has been modified to accept moving obstacle with each vehicle constituting a moving obstacle for the other vehicle. As can be seen in Figure 8, one of the vehicles autonomously and independently slows down so as to avoid UAV to UAV collision.

Figure 9 illustrates a navigation scenario where both moving and fixed navigation hazards are present. Here the navigation generator autonomously acts to simultaneously avoid both the fixed and moving obstacles.
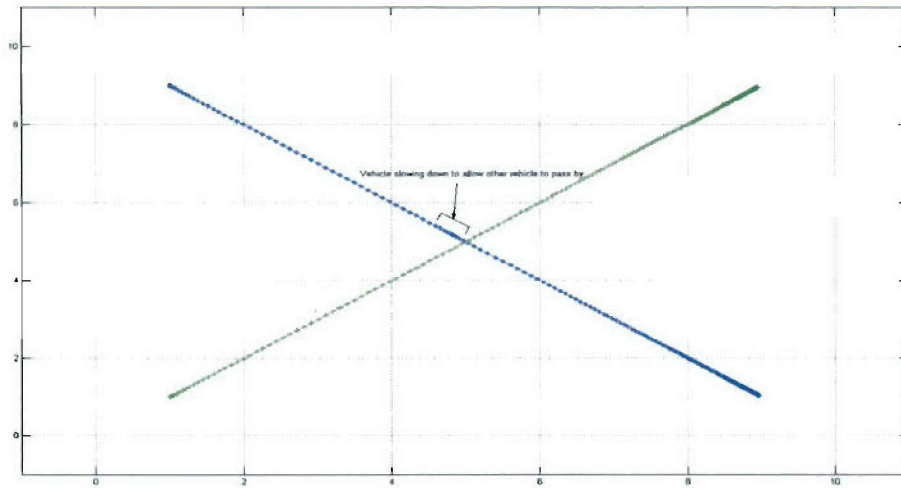
Figure 8: Navigational path with a moving obstacle

The generated trajectories are again smooth in position and velocity exhibiting monotonic synergistic convergence to target coordinates.
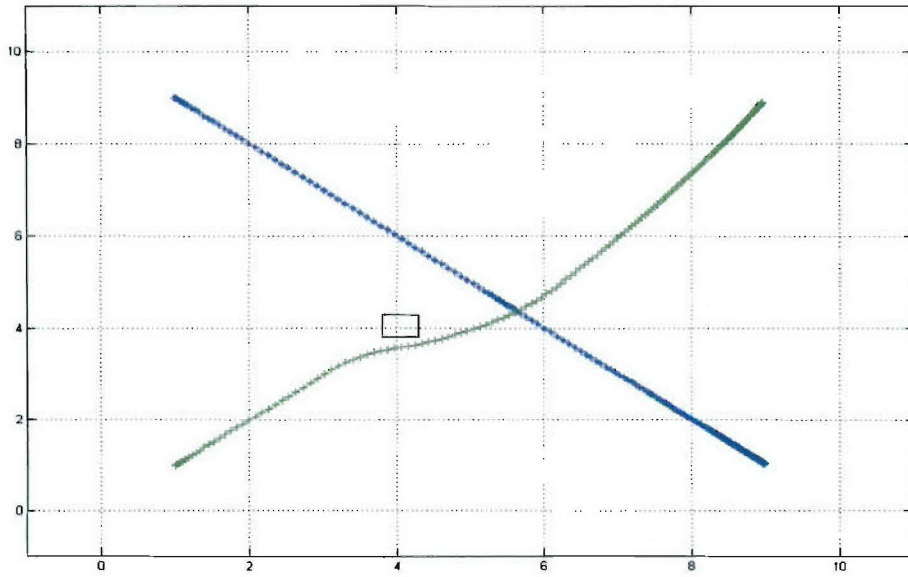
Figure 9: Navigational path with a fixed and moving obstacle

2.5.3.4 Pursuit and Interception

The interception of a moving target is a common navigation maneuver. This scenario is shown in Figure 10. In addition, if the intercepted target has sensing or defense capability it may be necessary to follow the target platform with a stand off distance.

This figure demonstrates inherent capability of the navigation generator to intercept a moving target while maintaining a safe stand-off distance. The simulation results of stand-off pursuit are given in Figure 11.
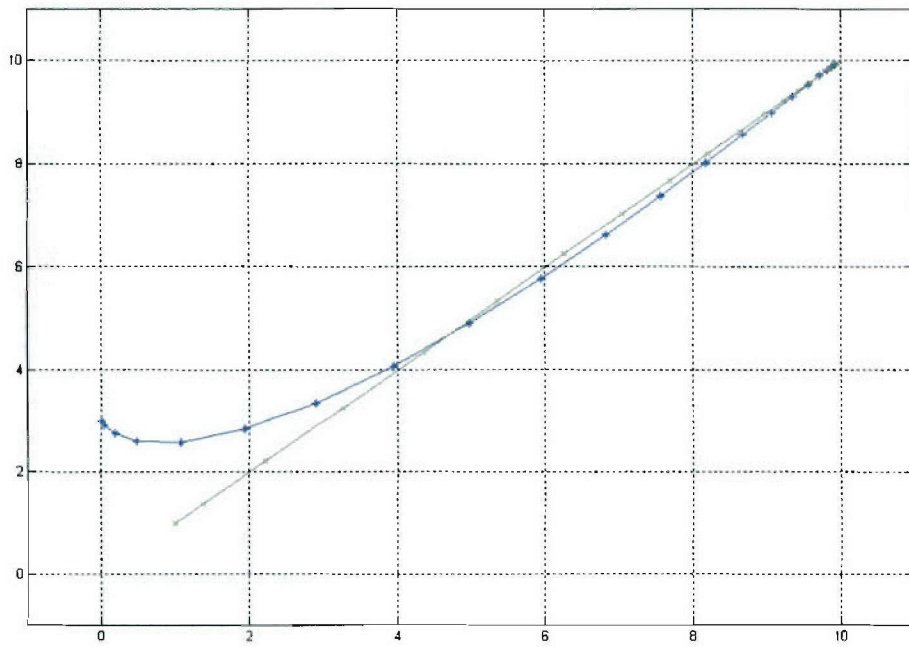
Figure 10: Moving target intercept navigational path
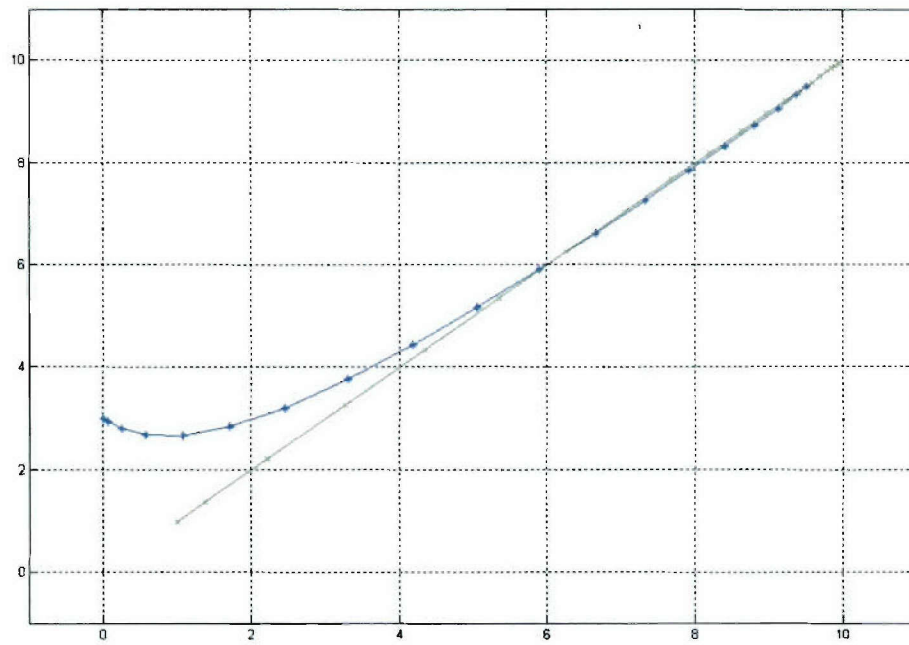
Figure 11: Moving target intercept with standoff

2.5.4 MIMO Real Time Model

A MIMO model was derived from Equations (1) and (2) for the purpose of allowing navigational computation to be interleaved with real-time sensing and communication. It also provides a means of fusing mission and navigation information as updated by communications information. In addition, a MIMO Real-time navigation model allows for the sequential processing of navigation, GPS and communication data in the computation of a neuro-fuzzy PIM. The baseline real time implementation of the MIMO sequential mode was accomplished first with communication links consisting of serial cables and simulated GPS position words. This scenario is described in the next section.

2.5.4.1 Real Time Performance & Emulation

The real time setup includes three computers; two slave computers and one master
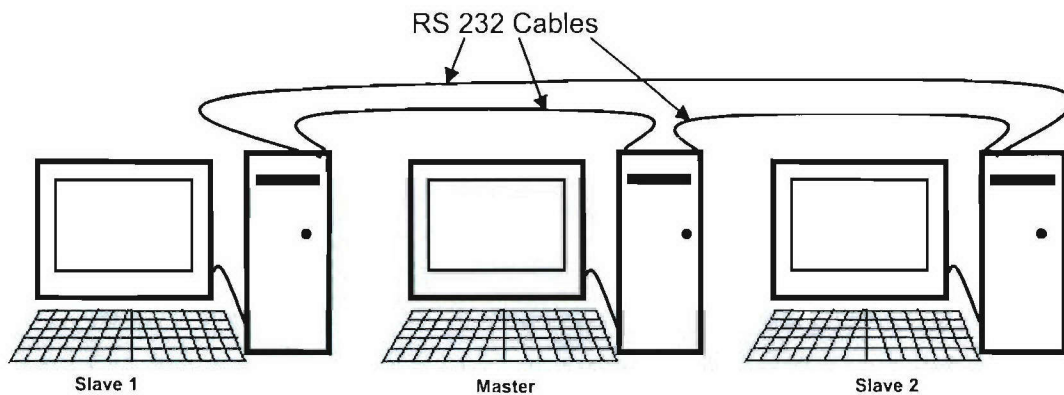
Figure 12: Set up for real time simulations

computer. The units are all connected by means of RS 232 cables. In the real-time setup both the slave computers wait for mission start up in addition to mission commands sent as targets and obstacles. The master station controls and monitors the mission progress.

2.5.4.1.1 Real Time Collision Avoidance

Once the mission commences Real-time collision avoidance is characterized by live communication link which, assumes that both slave computers provide their position coordinates to the master computer as well as to the other slave computer. The two slave computers autonomously navigate their respective UAV's in response to the location of the other UAV and the coordinates of mission targets. Figure 13 illustrates typical autonomous navigation results obtained during real-time navigation emulation for the typical case of UAV's with two obstacles in the direct path. In this case the desired final positions are communicated from the master station. The vehicle is observed to smoothly change its path depending on the position of the obstacles.
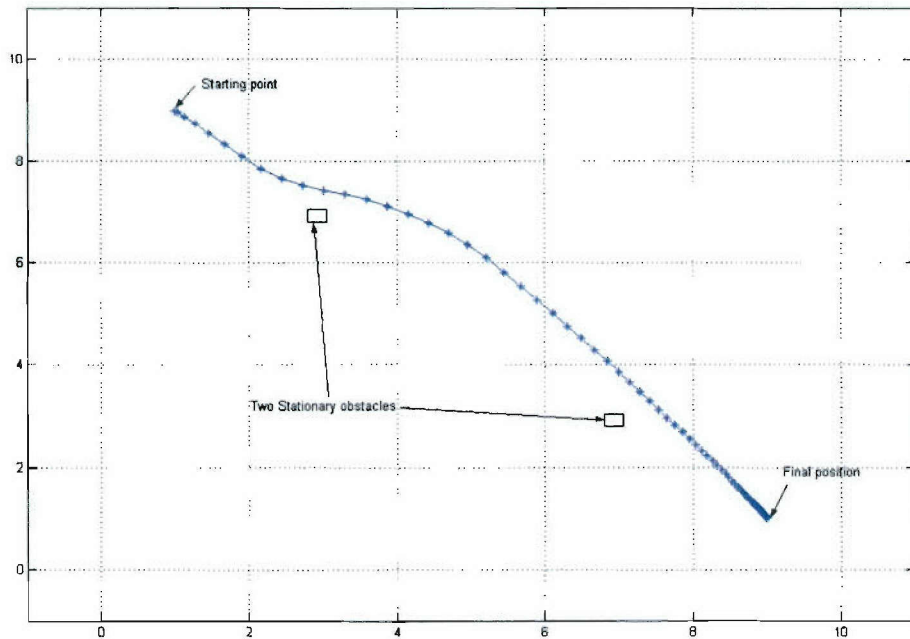
Figure 13: Real time navigation path with two obstacles

A real-time navigation case with two moving vehicles is presented next. In the real-time set up, motion of both the vehicles can be seen on the same plot at the master station. Figure 14 presents the real-time navigation emulation results. Both vehicles are observed to smoothly avoid both moving and fixed obstacles. All mission and obstacle data are communicated via serial ports and the resulting paths generated are non-oscillatory and monotonically convergent.
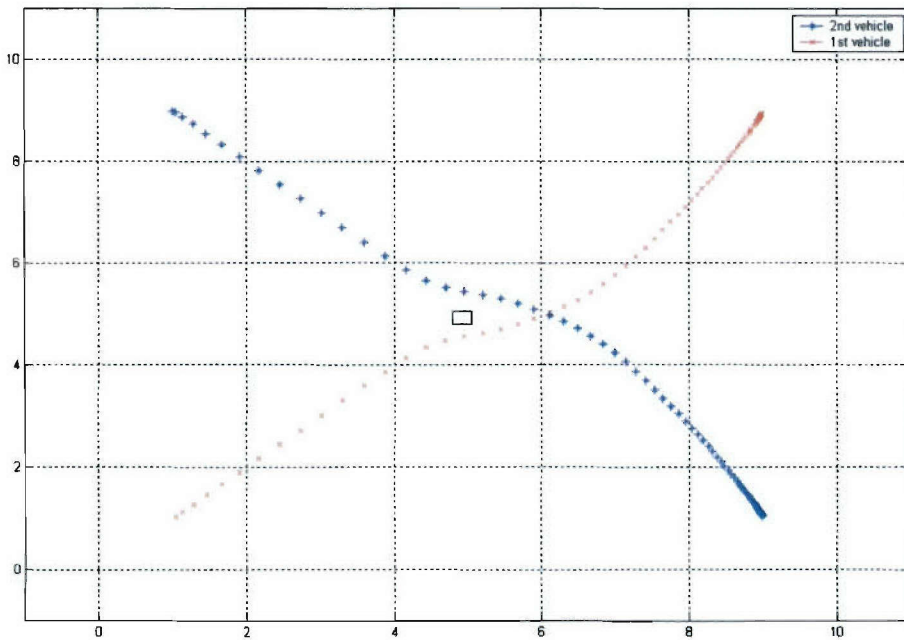
Figure 14: Plot of a real time navigational path with a fixed and moving obstacle (screenshot at master computer)

2.5.4.2 Real-Time Performance

The observed real-time performance indicates that the trajectory paths exhibit a fast ramp at start-up and a slow down as the final target is approached. The trajectories are stable, non-oscillatory, monotonic and smooth in position and velocity. Some nonsymmetry in

the smoothness was observed with accelerated initial start up and deaccelerated final approach to target.

2.6 Real Time Implementation Approach

The considerations in implementing the previously described real-time navigation generator with micro-controller and intelligent control is now addressed. From a broad perspective, the development of innovative technology aimed at reducing manning requirements and life cycle costs are driven by the Smart/Intelligent Ship philosophy evolved and adopted by the Navy for future platforms. The development of autonomous navigation control and information integration systems is anticipated to play a major role in this initiative. Within the framework of this initiative, the development of a methodology for the design and implementation of autonomous machinery control systems is proposed. The methodology must employ available COTS technology to provide a flexible integrated approach to accomplish the essential tasks of modeling, design, analysis, and assessment for shipboard environment/mission, prototyping and real-time implementation. An innovative feature of the proposed approach is that the previous task sequence is completely integrated into the final design implementation. The result is that all developmental expertise is retained within the controller and readily available for future use. The software structure also allows on-the-fly contingency assessment, parameter adjustment and supervisory operator training.

2.6.1 Considerations for Autonomous Machinery Control

The development of a flexible methodology for the integrated design and implementation of autonomous intelligent machinery control systems is proposed. The process of developing and deploying an intelligent autonomous navigation control system includes the following interrelated phases: (1) formulation of control objectives and strategy which incorporates component, system and shipboard wide intelligence capability; (2) modeling; (3) control algorithm analysis, design and assessment; (4) simulation; (5) rapid controller prototyping test and evaluation; (6) final implementation (distributed in COTS DSP based hardware with supervisory information integration). Considerations associated with each of these phases are discussed below.

2.6.1.1 Formulation of control objectives and strategy

The formulation of control objectives is driven by the need for any autonomously operated system to reconfigure itself to best support the mission of the platform. This includes anticipated modes of normal operation and damage control subject to overall ship status and immediate mission needs. In addition, the development of an intelligent decision structure is desirable in an attempt to provide reconfiguration capability under operational conditions resulting from unanticipated scenarios.

2.6.1.2 Modeling

Modeling is the essential fundamental process upon which control system analysis and design is based. Time and frequency domain models are based on an understanding of the physical processes that characterize the system components. These yield analytical and

numerical based approximate quantification of system component response. Component models may include the plant, associated sensors and actuator dynamics.

2.6.1.3 Simulation

Simulation provides the essential vehicle to integrate component models into a complete system model that also includes the controller. Closed loop simulations allow an assessment of how well the initial controller structure, and subsequent iterations of controller design, meet performance specifications.

2.6.1.4 Distributive controller design, assessment and algorithm

The framework for controller development is one of autonomous distributive control which is capable of adapting to numerous shipboard operational scenarios, anticipated and unanticipated, realizing a fight-while-hurt capability. The distributive control process incorporates: micro-controller component level intelligence; and system level intelligence via corroborative micro-controller components and PC based software. In addition, the control architecture must incorporate supervisory human direction with the potential to accept threat status and evasion information from combat systems, navigation, communication and damage control shipboard functions. The process of controller design is twofold. The first component is control strategy development and commonly involves a blend of approaches which include classical, modern, robust, μ-control, adaptive/predictive, intelligent, optimal, neural and fuzzy methods. The second component deals with implementation issues. Once a control algorithm is specified it must be encoded in a distributive environment consisting of series DSP based micro-

controllers. Consideration must be given to processor execution speed, I/O buffering, A/D and D/A conversion, and synchronization. From the distributive perspective issues of concern in best satisfying shipboard platform mission needs include the stand alone control action of individual micro-controllers in concert with corroborative control actions of micro-controller subsets.

2.6.1.5 Control algorithm prototype implementation and real-time testing

No matter how refined the model of an autonomous system is, it represents the result of an abstraction process and consequently there are physical phenomena that are not totally accounted for by the model. The model serves as the vehicle for bringing to bear the theoretically powerful analytical analysis and design approaches to the problem of developing an optimized automated machinery system. The resulting design is optimized with respect to the model representing the system and its validity in the framework of an actual hardware implementation must be addressed.

The conclusive performance assessment of a control algorithm lies in real-time implementation testing. This configuration consists of a physical plant, full or scaled, and in-the-loop controller hardware in addition to the implementation of supervisory software/hardware to assess and tune the control algorithm in real time. The supervisory software/hardware may also serve as a means to evaluate and optimize available control options subject to condition assessment, mission and human operator inputs.

3.0 DISTRIBUTRED DIVERSE SENSING

In the conventional array signal processing approach, the sensor locations must be separated by a maximum of one half wavelength of the dominant signal component in order to estimate the direction of arrival of acoustic source waves. This scenario is applicable to a sensor node containing a micro-array of acoustic sensors. In the case where the UAV sensor nodes contain single acoustic sensors and are separated by more than a half wavelength of the dominant acoustic frequency component, an augmented sensor processing problem results. The augmented sensor problem is illustrated in Figure 15. In this case the signal model cannot be directly employed to deduce source location information due to spatial sparsity. This may be overcome however, by employing the platform model dynamics, which augment the signal samples with a physical model of the propagation and acoustic environment. The augmented modeling cases, which were considered, include the sensor-to-sensor feature propagation delay augmentation and the hyper-geometric feature propagation delay augmentation. Geolocation and bearing technologies currently are rapidly evolving and the potential exists for employing these in extending the augmented location problem to a more autonomous state.
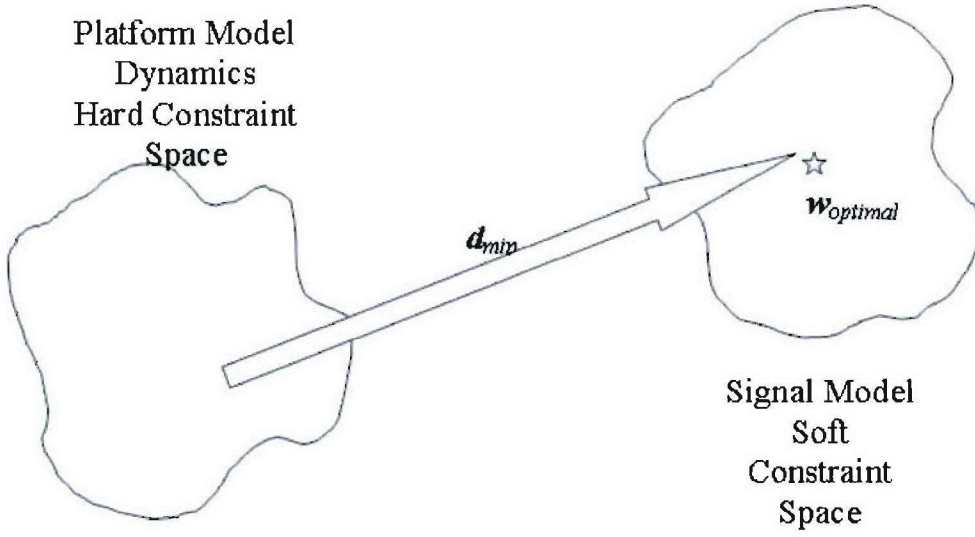
Figure 15: Framework of the augmented sensor array problem.

3.1 Sensor-to-sensor feature propagation delay

Propagation delay source location is characterized by sensor distributions that may be randomly distributed throughout a region without any restrictions on the distances between sensors in relation to the acoustic source wavelength [19], [26]. This is in contrast to phase based conventional sensor array processing techniques, which bound the spacing between sensors to within a half wavelength of the dominant frequency being analyzed for direction of arrival estimation. The typical geometric layout of the feature propagation approach is illustrated in Figure 16. The respective propagation delay times are given by:

$$\Delta T_{12} = T_2 - T_1$$
$$\Delta T_{13} = T_3 - T_1 \qquad (7)$$
$$\Delta T_{14} = T_4 - T_1$$

where T_1, T_2, T_3 and T_4 are the times of arrival at the corresponding sensors. The relative propagation delay between sensors of the source feature is used in concert with the coordinates of the acoustic sensor elements to determine the location of the acoustic source within the sensing region. Considering the source to have coordinates u and v, the equations of concentric circles about the source with radii of lengths corresponding to the various distances from the source to a respective sensor may be expressed as
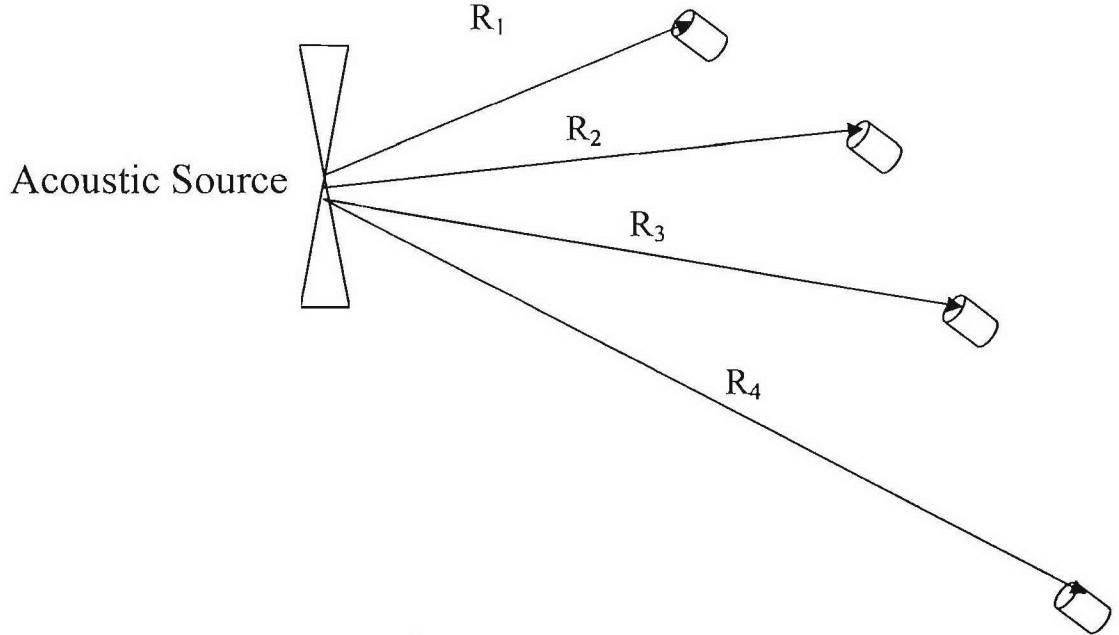
Figure 16: Sensor-to-sensor feature propagation delays.

$$(x_2 - u)^2 + (y_1 - v)^2 = (R_1)^2$$
$$(x_2 - u)^2 + (y_2 - v)^2 = (R_1 + s\Delta T_{12})^2$$
$$(x_3 - u)^2 + (y_3 - v)^2 = (R_1 + s\Delta T_{13})^2 \cdot$$
$$(x_4 - u)^2 + (y_4 - v)^2 = (R_1 + s\Delta T_{14})^2$$

(8)

Equation (8) may be rearranged into the matrix form as

$$\begin{bmatrix} 2x_1 - 2x_2 & 2y_1 - 2y_2 & -2v\Delta T_{12} \\ 2x_1 - 2x_3 & 2y_1 - 2y_3 & -2v\Delta T_{13} \\ 2x_1 - 2x_4 & 2y_1 - 2y_4 & -2v\Delta T_{14} \end{bmatrix} \begin{bmatrix} u \\ v \\ R_1 \end{bmatrix} = \begin{bmatrix} v^2\Delta T_{12}^2 + x_1^2 + y_1^2 - x_2^2 - y_2^2 \\ v^2\Delta T_{13}^2 + x_1^2 + y_1^2 - x_3^2 - y_3^2 \\ v^2\Delta T_{14}^2 + x_1^2 + y_1^2 - x_4^2 - y_4^2 \end{bmatrix}$$

(9)

The matrix equation (9) may be directly solved to yield $\begin{bmatrix} u \\ v \\ R_1 \end{bmatrix}$ and requires a minimum of

four acoustic sensors. This method is may be extrapolated to three dimensions and requires a minimum of five non-collinear acoustic sensors to achieve an estimate of the source coordinates.

3.2 Hyper-geometric feature propagation

The hyper-geometric characterization of source location with respect to a constellation of acoustic sensors is illustrated in Figure 17. In contrast to the four sensors required by the feature time delay approach for 2-D source location estimation, the hyper-geometric approach requires only three sensors, which are non-collinear. In the case of 3-D source coordinate estimation, the hyper-geometric approach requires four non-collinear acoustic sensor vice the five non-collinear sensors required by the feature propagation delay approach. The hyper-geometric approach consists of simultaneously solving for the intersection of two, 2-D case, or three, 3-D case, hyper curves. The appropriate curves are

selected based on the time of arrival of the acoustic wave at the various sensors. In the 2-D case the two sensors with the first two arrival times are chosen as the corresponding foci of hyper-geometric curves. In the three dimensional case the three sensors with the first three arrival times are chosen as the reference foci. Without loss of generality, the hyper-geometric method may be characterized for the case of sensors symmetrically located about the origin. Let the lattice rectum intersect the x-axis at c and $-c$, which are foci. These curves are characterized by

$$\frac{x^2}{a_x^2} - \frac{y^2}{c_x^2 - a_x^2} = 1 \tag{10}$$

In the analogous case of focii on the y-axis at c and $-c$, the corresponding curves are represented by

$$\frac{y^2}{a_y^2} - \frac{x^2}{c_y^2 - a_y^2} = 1 \tag{11}$$
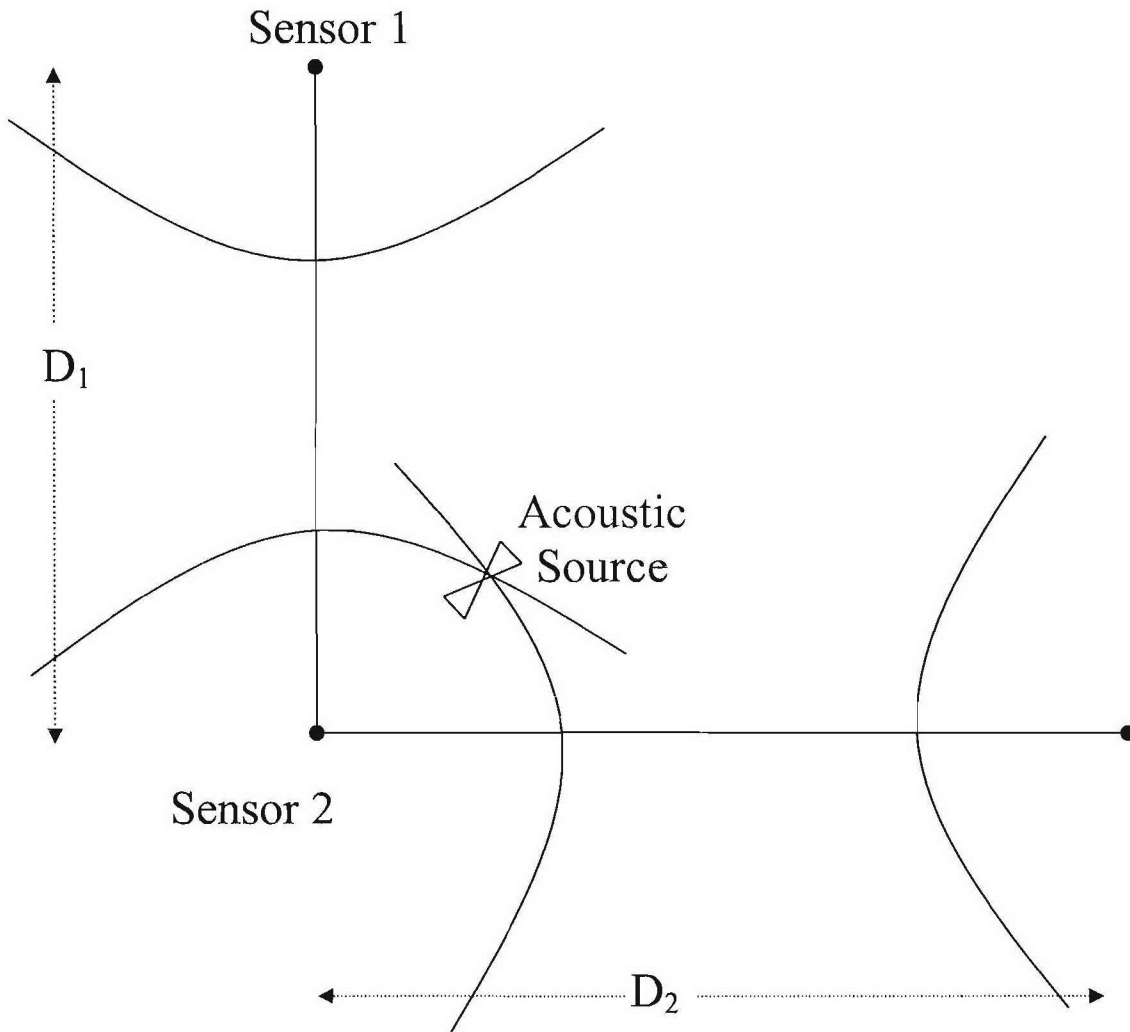
Figure 17: Hyper-geometric feature propagation delay sensor geometry.

The quantities a_y and a_x are the y and x-axis intercepts as derived from a fusion of the relative sensor-to-sensor time delays. Furthermore, the intersection between these sets of curves may be expressed as

$$x^2 = \frac{\left(b_x^2 + a_y^2\right)}{\left(\dfrac{b_x^2}{a_x^2} - \dfrac{a_y^2}{b_y^2}\right)} \tag{12}$$

and

$$y^2 = \frac{\left(b_y^2 + a_x^2\right)}{\left(\dfrac{b_y^2}{a_y^2} - \dfrac{a_x^2}{b_x^2}\right)} \tag{13}$$

where

$$b_x^2 = c_x^2 - a_x^2 \tag{14}$$

and

$$b_y^2 = c_y^2 - a_y^2 \tag{15}$$

The generalized coordinate case is derived from the above symmetric development by incorporating applicable rotational and transnational operators on the corresponding 2-D or 3-D coordinate n-tuple. The localization process requires only the extraction of the applicable a_x, a_y or a_z from the sampled acoustic data. Thus yielding a reduction in the required number of sensors required in contrast to the direct feature propagation delay methodology.

3.3 DISTRIBUTED SHIPBOARD APPLICATION

The fundamental problem of autonomous intelligent control for distributed fluid systems is addressed as an initial target application. Modeling, simulation and control methodologies are considered for leak damage detection, leak isolation and resource optimization in meeting load demand. While the results are primarily applied to UAV distributed systems, they extend directly to a wide range of sensors and deployment sensors.

3.3.1 System Configuration

A representative low-pressure (LP) system configuration is illustrated in Figure 18. The
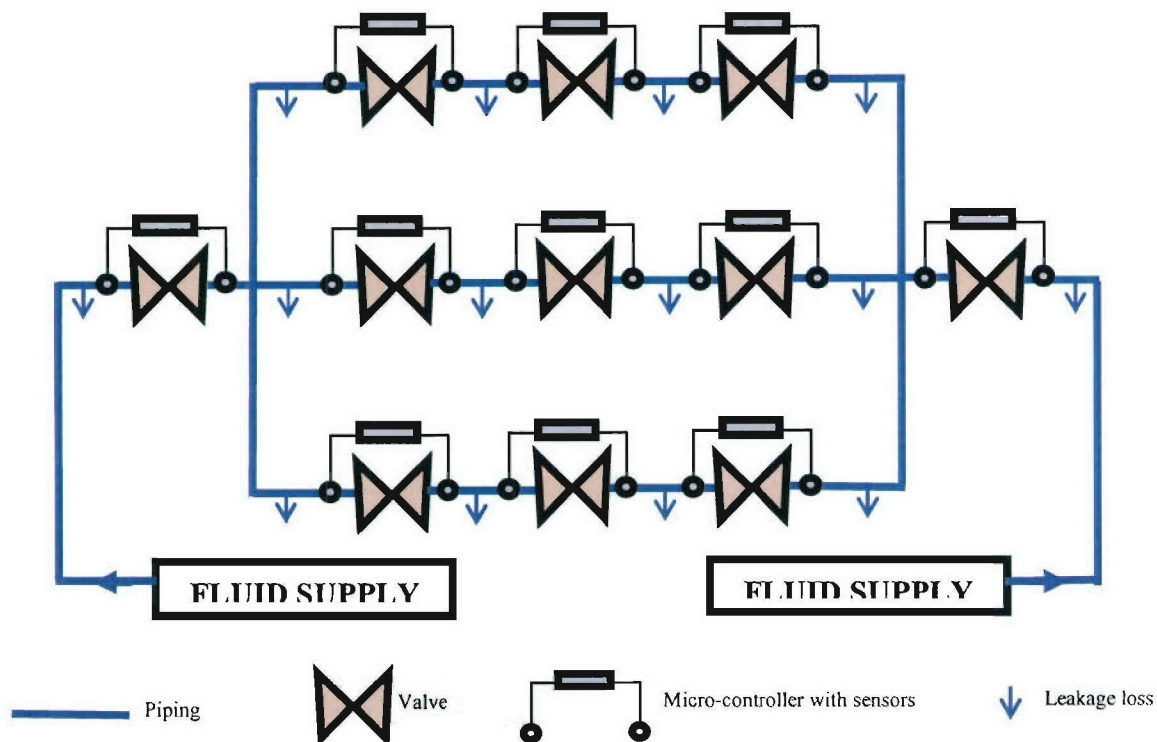
Figure 18: A typical UAV system series-parallel network configuration.

topology of the system consists of a series-parallel fluid flow network composed of piping sections, valves, sensors, micro-controllers and fluid supplies. The fluid supply units feed the network and consist of a motor-driven regulated compressor unit, a filter unit and a dehydration baffle. The piping sections contain automated on/off flow valves whose control actions are dictated by a dedicated micro-controller unit. The micro-controller units each employ a locally programmable control algorithm driven by the readings of two pressure switch sensors located on either side of the valve unit. Thus, a micro-controller operates its valve unit in accordance with an assessment of the pressure state of system piping on both sides of the valve. In addition, each of the piping sections and/or valve units may experience a leakage failure. Under normal and failure operating conditions, the fundamental goal is to achieve optimal autonomous operation in meeting the system load demand.

3.3.2 Distributed Failure Problem Statement

The problem focus is one of developing a distributed control methodology with the objective of achieving optimized autonomous operation. The major aspect of this problem is how to allocate the available capability of the UAV supply to best satisfy load demands. This includes supplying load demands under normal operation and subject to anticipated and unanticipated system damage scenarios. The system component damage may include any combination of: (1) moderate leakage failures in piping and valve components; (2) catastrophic leakage failures in piping and valve components; (3) stuck valve failure; (4) partial/total failure of communication between micro-controller units (5) gradual component deterioration.

3.3.3 Approach

The approach taken in addressing the stated problem consists of: (1) a characterization of the dominant physical phenomena within the system; (2) analytical component model development; (3) simulation component model development in conjunction with micro controller action modeling; (4) a characterization of the existing pressure propagation distributed control methodology; (5) suggestions for incorporation into the existing control methodology; (6) a summary of potential concepts and approaches for hardware, software and distributed control methodology development.

3.4 ANALYTICAL MODEL DEVELOPMENT

The models considered include the non-dynamic and lumped dynamic cases. The efficacy of extending the models to the more complex spatially distributed parameter dynamic forms is contingent on experimental validation results for the non-dynamic and lumped parameter dynamic models.

3.4.1 Analytical Non-Dynamic Propagation Delay Model

A fundamental wave propagation model is developed for the case of catastrophic pipe leakage failure. Consider an UAV airline of diameter d_{lp} meters that is fed from a compressor incorporating a series combination of a debris filter and a dehydrator baffle. The effective restrictive diameter of the filter/baffle combination is denoted d_{fb} and it is assumed that $d_{fb} << d_{lp}$. Furthermore, let the UAV airline incur a large cross-sectional damage failure of area $a_f >> \pi d_{lp}$ square meters. Under the prescribed failure conditions,

a simplified plug-flow pressure wavefront is assumed to characterize the depressurization propagation process through the pipeline. The plug-flow process neglects viscous friction and assumes that the delay in propagation, i.e. propagation velocity, is the result of inertia. Under plug-flow conditions the pressure distribution $p(x,t)$ at a point $x \gg a_f$ meters away from the centroid of the damage fault may be expressed the relation

$$p(x,t) = \begin{cases} p_O & \text{for } x < v_p \text{t} \\ 0 & \text{for } x > v_p \text{t} \end{cases} \qquad (16)$$

where v_p is the plug flow propagation velocity in meters per second. The function $p(x,t)$ may be expressed in terms of the unit step function $u(\tau)$ by

$$p(x,t) = p_O u(x - v_p t) \qquad (17)$$

where

$$u(\tau) = \begin{cases} 0 \text{ for } \tau < 0 \\ 1 \text{ for } \tau > 0 \end{cases} \qquad (18)$$

The propagation of a pressure waveform through a piping section according to the inertial propagation delay model is illustrated in Figure 19.
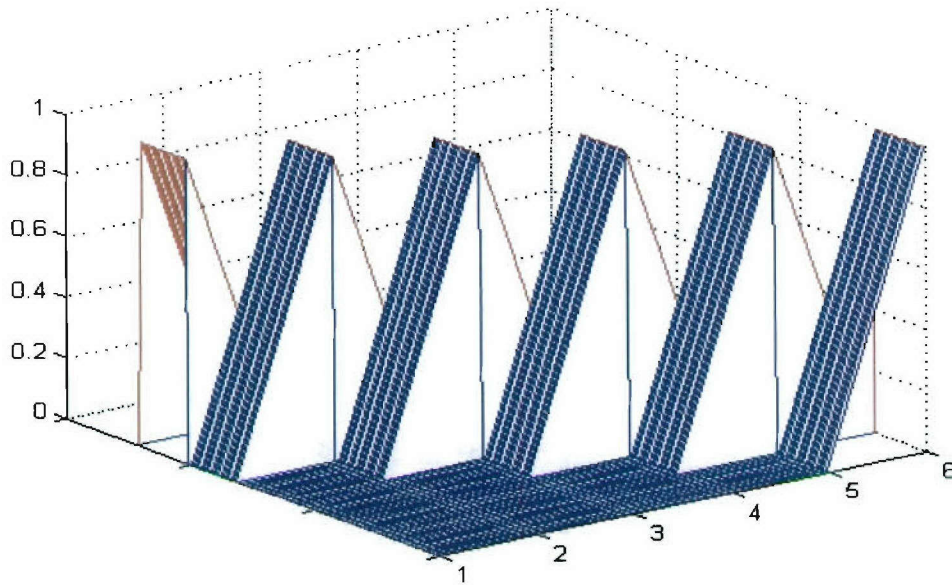
Figure 19: The propagation of unit amplitude ramped pulse through a piping section with a dwell time of six seconds.

3.4.2 Analytical Lumped Fluid Flow Model

The lumped parameter model developed incorporates fluid viscosity and compressibility through Poiseuille's law and the ideal gas law respectively. The development considers the case of incompressible flow, which is plausibly applicable for a wide range of commonly encountered air operating velocities.

3.4.2.1 Mach Number

Compressible and incompressible fluid flow velocity ranges

The speed of sound in a gas medium is given by

$$c = \sqrt{kRT} \tag{19}$$

where k is the ratio of specific heat at constant pressure to specific heat at constant volume ($k=1.4$ for air), R is the universal gas constant and T is the absolute temperature. The velocity of sound in air at *STP* is approximately 343 *m/s*,. The Mach number is given by the ratio

$$M = \frac{v}{c} \tag{20}$$

where c is the speed of sound and v is the flow velocity of the **gas**. A gas flow with a Mach number of 0.3 or less, at standard conditions, corresponds to gas flow velocities less than 100 m/s and this condition has been approximated as incompressible flow [22]. In situations where the Mach number is greater than 0.3, the gas density variation must be accounted for.

3.4.2.2 Viscous fluid characteristics

The internal friction associated with a fluid is characterized by viscosity. This well-known property gives fundamental insight into the mechanism of the prominent aspects of fluid behavior and a summary of an approach to its development is given, [7], [22], [25]. In laminar flow, the motion of a fluid is considered to consist of layers of fluid sliding past each other. The fluid viscosity results in a frictional coupling between adjacent layers of fluid. Consequently, a force must be exerted between adjacent layers if they move past each other. One of the classic examples of viscous flow is that of two parallel plates with a fluid channel separating them. This situation is shown in Figure 20 where Plate 1 is moving with velocity v relative to Plate 2 that is stationary. The fluid adjacent to Plate 2 travels with velocity v while the fluid adjacent to Plate 2 has velocity zero. The fluid velocity profile in the y-direction is considered to be distributed among a

set of thin fluid sheets, i.e. lamina, which slide across each other. The laminas interact and transmit force via the viscosity of the fluid. In order to maintain the motion of Plate 1 a force must be continually applied to this plate. The force applied to Plate 1 is transmitted to plate 2 through the viscous interaction of an infinite series of laminar sheet flows. The viscosity therefore is a measure of the fluid's resistance to flow.

If Plate 1 has area A, and the horizontal force applied to this plate is F, experimental measurements with Newtonian fluids show that the force required to maintain the velocity of Plate 1 is proportional to the velocity and plate area, while being inversely proportional to the plate separation x, [22]:

$$F \propto \frac{dv}{dt} \frac{A}{X} \tag{21}$$

The constant of proportionality is known as absolute viscosity. The terms in equation (21)
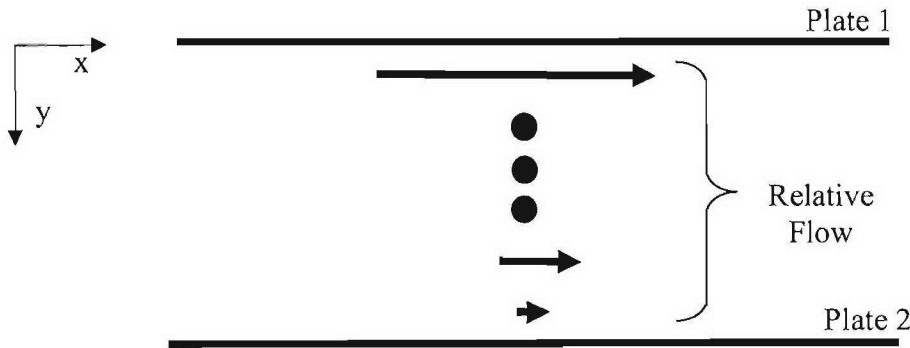
Figure 20: Illustration of relative velocity distribution for parallel plate laminar flow.

give rise to various definitions of quantities describing fluid physical properties. The shear stress exerted on the fluid is defined as

$$Shear\ stress = \frac{F}{A} \qquad (22)$$

When a shear stress is applied to a solid material, the result is a displacement along the vertical dimension, with respect to the configuration of force shown in Figure 20. Shear strain is the ratio of the resultant displacement dy to the transverse dimension X and is defined as

$$Shear\ strain = \frac{dy}{X} \qquad (23)$$

In the case of a fluid, shear strain increases without limit as long as a shear stress is applied. In this case, the shear stress is related to the rate of change of the shear strain. The rate of change of shear strain is defined as

$$Strain\ rate = \frac{v}{X} \qquad (24)$$

Furthermore, the viscosity of a fluid is defined as the ratio of shear stress to strain rate and is denoted by

$$\eta = \frac{Strain\ rate}{Shear\ stress}$$
$$= \frac{F/A}{v/X} \qquad (25)$$

and equation (21) may be expressed as

$$F = \eta A \frac{v}{X} \qquad (26)$$

The *MKS* units of viscosity are *N-s-m^{-2}*. The practical measure of viscosity is the poise where 1 one poise has *MKS* units of *(N-s-m^{-2})×10^{-1}*. The viscosity of air at an ambient temperature of 20°C is 181×10^{-6} poise or 181μ-poise.

3.4.2.3 Poiseuille's Law of viscous flow

As a viscous fluid flows within a tube its velocity varies across the cross-section of the tube. The velocity distribution is zero at the wall and increases to a maximum value at the center of the tube. The wall of the tube exerts a drag on the outermost layer of the fluid and this layer on the next layer and so on and, if the flow is laminar, the maximum velocity occurs along the center of the tube. In effect, this may be viewed as a series of concentric cylindrical surfaces sliding across each other.

3.4.2.3.1 Flow velocity

Consider a pipe of circular cross-section with radius R and length L. Let pressure p_1 be applied to the left side of the pipe and pressure p_2 applied to the right side. Consider a cylindrical fluid volume within the pipe of radius $r \leq R$ which is centered along the pipe axis, the net force F exerted on the fluid within this volume is the difference between the forces applied at the ends of this pipe subsection:

$$
\begin{aligned}
F &= p_1 \pi r^2 - p_2 \pi r^2 \\
&= (p_1 - p_2)\pi r^2
\end{aligned}
\tag{27}
$$

In steady state, the velocity profile is time invariant and consequently the force applied to the fluid just balances the viscous retarding force generated within the fluid at the operating steady-state velocity. In the case where the velocity is uniform over the pipe cross-section, force is related to viscosity by equation (26)

In actuality the fluid velocity is not uniform and varies as a function of the radius r. In this case, the relationship between force and viscosity for a cylindrical sheet of length L, radius r and thickness dr follows from (26):

$$
F = \eta 2\pi r L \frac{dv}{dr}.
\tag{28}
$$

where $\frac{v}{X}$ is replaced with $\frac{dv}{dr}$ and A is replaced by $2\pi r L$. Equating the force in equation (27) to that of equation (28) yields the relationship

$$\frac{dv}{dr} = -\frac{(p_1 - p_2)r}{2\eta L} \tag{29}$$

which indicates that the velocity gradient, with respect to the pipe radius, changes more and more rapidly as the radius increases. Equation (29) is separable and characterizes the velocity profile as

$$-\int_v^0 dv = \frac{(p_1 - p_2)}{4\eta L} \int_r^R r\,dr \tag{30}$$

which gives

$$v = \frac{(p_1 - p_2)}{4\eta L}(R^2 - r^2) \tag{31}$$

The velocity is bounded by $0 \le v \le \frac{(p_1-p_2)R^2}{4\eta L}$ with a maximum value at the center of the pipe and a zero velocity at the pipe wall. The velocity is proportional to $(p_1 - p_2)/L$ the pressure gradient, i.e. the change in pressure per unit length of pipe.

3.4.2.3.2 Total rate of volumetric flow

Consider a very thin cylindrical surface section of fluid whose major axis is concentric with that of a circular piping line. Let the inner radius of the fluid cylinder be denoted by r, and its thickness by dr. The volume dV_{VOL} crossing the end area of the fluid cylinder over a time interval dt is $dV_{VOL} = v \times dA \times dt$ where the area A is equal to $2\pi r dr$.

Substituting equation (31) for the velocity v gives

$$dV_{VOL} = \frac{(p_1 - p_2)}{4\eta L}(R^2 - r^2)2\pi r dr dt \qquad (32)$$

Integrating across the entire pipe cross-section gives and expression for the net volumetric fluid flow which is given by

$$dV_{VOL} = \frac{\pi(p_1 - p_2)}{2\eta L}\int_0^R (R^2 - r^2)r dr dt \qquad (33)$$

or

$$\frac{dV_{VOL}}{dt} = \frac{\pi}{8}\left[\left(\frac{R^4}{\eta}\right)\left(\frac{p_1 - p_2}{L}\right)\right] \qquad (34)$$

The volumetric flow relationship in (34) is referred to as Poiseuille's law [22].

3.4.2.4 Vessel ideal gas equation of state

Assuming an instantaneous gas fluid equilibrium not subject to influence of motion, shear, body force, stress and capillary action; the equation of state for a gas is given by the well-known expression

$$pV = nRT \qquad (35)$$

where R is the universal gas constant having a value of 8.314 J-mol^{-1}-K^{-1}, T is the absolute temperature, V_{VOL} is the volume, p is the pressure, and n is the number of moles of the gas [1]. The number of moles of gas, n, is related to the total mass, m, of the gas by $n = {}^m\!/_M$ where M is the mass per mole. Thus (35) may be expressed in terms of mass as:

$$pV_{VOL} = \frac{m}{M} RT \qquad (36)$$

3.4.3 Single-ended state of flow model

Consider the case of a gas vessel being fed through an orifice effectively acting as a feed
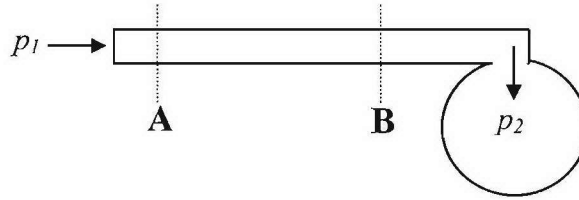
Figure 21: Pipe section lumped vessel model subject to only one end-valve open.

pipe. This situation corresponds to a pipe section with one end-valve open and the other end-valve closed as depicted in the Figure 21. The pipe section is driven by an applied pump pressure p_1 and this causes a fluid mass flow into the vessel whose internal fluid pressure is given by $p_2 \leq p_1$. Under conditions of steady flow, the continuity of mass flow satisfies

$$\dot{m} = \left.\frac{Av}{v_{sp}}\right|_A = \left.\frac{Av}{v_{sp}}\right|_B = \left.\frac{Av}{v_{sp}}\right|_{At\ any\ cross\ section} \qquad (37)$$

where v denotes flow velocity, A is the pipe cross-sectional area perpendicular to the direction of fluid velocity, and v_{sp} is fluid specific volume. Substituting equation (37) into Poiseuille's law (34), and recalling that $dV_{VOL} = v \times dA \times dt$ yields the following expression for mass flow rate:

$$\dot{m} = \frac{dV_{VOL}}{dt} \left(\left. \frac{1}{v_{sp}} \right|_A \right)$$
$$= \frac{\pi}{8} \left[\left(\left. \frac{1}{v_{sp}} \right|_A \right) \left(\frac{R^4}{\eta} \right) \left(\frac{p_1 - p_2}{L} \right) \right]$$

(38)

For gases at a constant temperature

$$\left. pv_{sp} \right|_A = \left. pv_{sp} \right|_B = \left. pv_{sp} \right|_{Any\ cross\ section} = \frac{m}{M} RT$$

(39)

and furthermore, under constant temperature:

$$p_2(t) = \left[\frac{MRT}{V_{VES}} \right] m(t)$$

(40)

Equations (39) and (40) may be respectively expressed as

$$\dot{m}(t) = R_{EQ} (p_1(t) - p_2(t))$$

(41)

51

and

$$p_2(t) = C_{EQ}m(t) \tag{42}$$

where R_{EQ} represents and equivalent pipe flow resistance given by

$$R_{EQ} = \left[\left(\frac{1}{v_{sp}} \bigg|_A \right) \left(\frac{R^4}{\eta} \right) \left(\frac{1}{L} \right) \right] \tag{43}$$

and C_{EQ} represents and equivalent vessel capacitance given by

$$C_{EQ} = \left[\frac{MRT}{V_{VES}} \right] \tag{44}$$

3.4.3.1 Analytical lumped parameter lossless single end-valve model

Substituting equation (41) into (42) yields a lumped parameter differential relationship which describes a steady-flow pressurization and de-pressurization of the pipe chamber vessel model:

$$\dot{m}(t) = R_{EQ}(p_1(t) - C_{EQ}m(t)) \tag{45}$$

Rearranging (45) gives

$$\dot{m}(t) + C_{EQ}R_{EQ}m(t) = R_{EQ}p_1(t) \tag{46}$$

The pressure function $p_l(t)$ acts as an input or forcing function to the pipe-vessel system while $m(t)$ is the output or system response. The transfer function of the system is arrived at by taking the Laplace transform of the differential equation (46) subject to zero initial conditions [2], [4]. This yields

$$\frac{\dot{M}(s)}{P_1(s)} = \frac{R_{EQ}}{\left(s + R_{EQ} C_{EQ} \right)} \tag{47}$$

The electrical analog circuit is shown in Figure 22 depicts the charging of a vessel due to a pressure $p_l(t)$ applied through one end of the pipe.
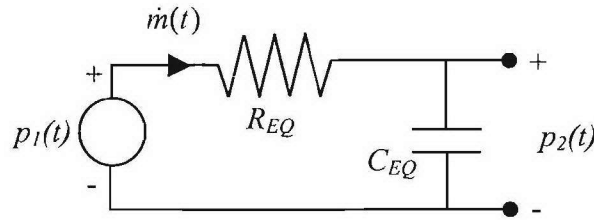
Figure 22: Electrical analog to a lossless pipe with only one end-valve open.

3.4.3.2 Analytical lumped parameter lossy dual end-valve model

The presence of a leak precipitates a discharge flow that reduces the pressure level within a section of piping. The impact of a leak is introduced via an analogous resistive shunting section across the equivalent vessel capacitance as shown in Figure 23. The piping section pressure, $p_2(t)$, is a function of the pressure, $p_l(t)$, generated by the compressor pump(s) and the leakage rate.

The piping vessel pressure as a function of the pumping pressure and leakage rate is given by the transfer function
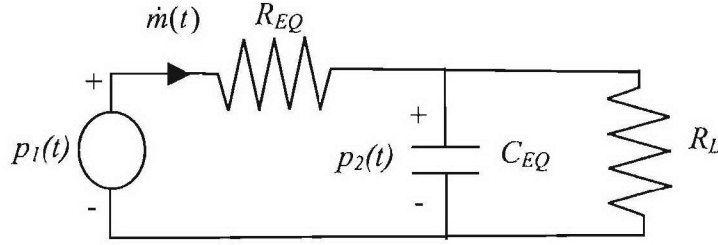
Figure 23: Electrical analog to a lossy pipe with only one end valve open.

$$\frac{P_2(s)}{P_1(s)} = \frac{\dfrac{R_L}{1+sR_LC_{EQ}}}{R_{EQ}+\dfrac{R_L}{1+sR_LC_{EQ}}} = \frac{R_L}{R_{EQ}\left(1+sR_LC_{EQ}\right)+R_L}$$

$$= \frac{R_L}{\left(R_L+R_{EQ}\right)+s\left(R_{EQ}R_LC_{EQ}\right)} \tag{48}$$

3.4.4 Dual-ended state of flow model

A transmission pipe within the system will generally receive a supply of fluid from either end as shown in Figure 24. This may be the consequence of the system being supplied by multiple compressors and/or as a consequence of internal piping loops present within the system. Figure 25 illustrates the electrical analog of the piping system with both end-valves open in conjunction with fluid loss piping damage.
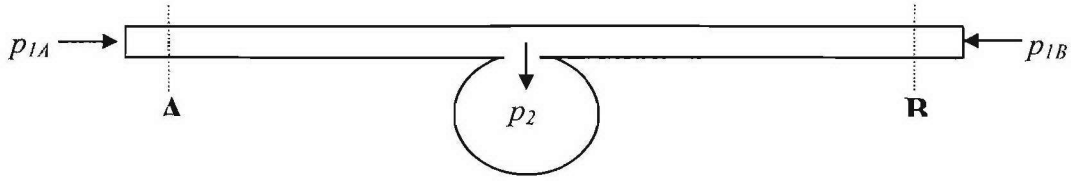
Figure 24: Pipe section lumped vessel model subject to both end-valves open.

The mass flow rates and the vessel pressure are related to the compressor driving pressures and piping loss by the Laplace domain matrix equation:

$$\begin{bmatrix} P_{1A}(s) \\ P_{1B}(s) \end{bmatrix} = \begin{bmatrix} R_A + Z_{EQ} & -Z_{EQ} \\ -Z_{EQ} & R_B + Z_{EQ} \end{bmatrix} \begin{bmatrix} \dot{M}_A(s) \\ \dot{M}_B(s) \end{bmatrix} \qquad (49)$$
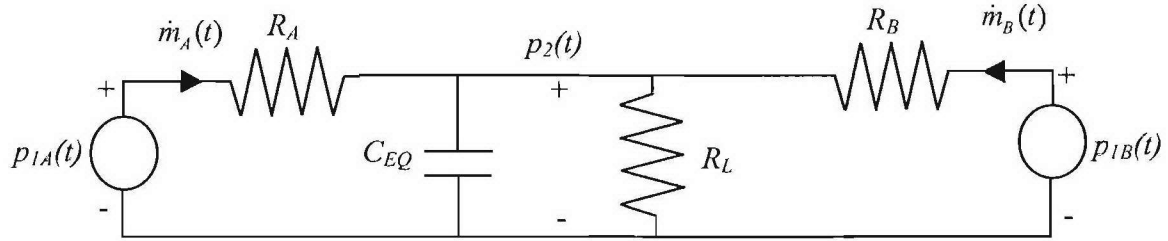
Figure 25: Electrical analog to a lossy pipe with both end-valves open.

where

$$Z_{EQ} = Z_{C_{EQ}} \| R_L |$$
$$= \frac{R_L}{1 + sC_{EQ}R_L} \qquad (50)$$

Solving (49) for the mass flow rates gives

$$
\begin{bmatrix} \dot{M}_A(s) \\ \dot{M}_B(s) \end{bmatrix} = \frac{\begin{bmatrix} R_A + Z_{EQ} & -Z_{EQ} \\ -Z_{EQ} & R_B + Z_B \end{bmatrix}}{R_A R_B + (R_A + R_B) Z_{EQ}} \begin{bmatrix} P_{1A}(s) \\ P_{1B}(s) \end{bmatrix}
\tag{51}
$$

The vessel pressure is given by

$$
\begin{aligned}
P_2(s) &= Z_{EQ}(\dot{M}_1(s) + \dot{M}_2(s)) \\
&= Z_{EQ}\left(\frac{R_A P_{1A}(s) + R_B P_{1B}(s)}{R_A R_B + (R_A + R_B) Z_{EQ}} \right) \\
&= \frac{R_L\left(\dfrac{R_A R_B}{R_A + R_B} \right)\left[\dfrac{R_L}{R_B} P_{1A}(s) + \dfrac{R_L}{R_A} P_{1B}(s) \right]}{\left[\dfrac{R_A R_B}{R_A + R_B} + R_L \right] + s\left[C_{EQ} R_L\left(\dfrac{R_A R_B}{R_A + R_B} \right) \right]}
\end{aligned}
\tag{52}
$$

For the case where $R_A = R_B = R_{EQ}$,

$$
\begin{bmatrix} P_{1A}(s) \\ P_{1B}(s) \end{bmatrix} = \begin{bmatrix} R_{EQ} + Z_{EQ} & -Z_{EQ} \\ -Z_{EQ} & R_{EQ} + Z_{EQ} \end{bmatrix} \begin{bmatrix} \dot{M}_A(s) \\ \dot{M}_B(s) \end{bmatrix}
\tag{53}
$$

where

$$
\begin{aligned}
Z_{EQ} &= Z_{C_{EQ}} \parallel R_L \\
&= \frac{R_L}{1 + s C_{EQ} R_L}
\end{aligned}
\tag{54}
$$

Solving equation (53) for the mass flow rates gives

$$
\begin{bmatrix} \dot{M}_A(s) \\ \dot{M}_B(s) \end{bmatrix} = \frac{\begin{bmatrix} R_{EQ} + Z_{EQ} & -Z_{EQ} \\ -Z_{EQ} & R_{EQ} + Z_{EQ} \end{bmatrix}}{R_{EQ}\left(R_{EQ} + 2Z_{EQ}\right)} \begin{bmatrix} P_{1A}(s) \\ P_{1B}(s) \end{bmatrix} \tag{55}
$$

Combining equations (54) and (55) yields and expression for the bi-directional lossy flow transfer function

$$
\begin{aligned}
P_2(s) &= Z_{EQ} \times \left(\dot{M}_A(s) + \dot{M}_B(s)\right) \\
&= \frac{1}{\left(2 + \dfrac{R_{EQ}}{Z_{EQ}}\right)}\left(P_{1A}(s) + P_{1B}(s)\right) \\
&= \frac{R_L}{(2R_L + R_{EQ}) + sC_{EQ}R_L}\left(P_{1A}(s) + P_{1B}(s)\right)
\end{aligned} \tag{56}
$$

which may be expressed in terms of a multi-input transfer function matrix, $\mathbf{H}(s)$, as

$$
[P_2(s)] = \mathbf{H}(s)\begin{bmatrix} P_{1A}(s) \\ P_{1B}(s) \end{bmatrix} \tag{57}
$$

where

$$
\mathbf{H}(s) = \left[\left(\frac{1}{2 + \dfrac{R_{EQ}}{Z_{EQ}}}\right), \left(\frac{1}{2 + \dfrac{R_{EQ}}{Z_{EQ}}}\right)\right] \tag{58}
$$

57

3.4.5 Isolation state model for both end-valves closed

The remaining response scenario to be addressed is the situation in which both end valves of a pipe section are closed. In this case the pressure remains constant or, if a leak is present, decays exponentially. The vessel pressure $p_2(t)$ is characterized by the circuit analog shown in Figure 26.
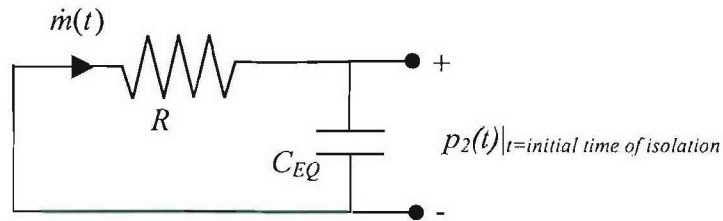
Figure 26: Electrical analog to a lossy pipe with both end-valves closed.

From the instant that both valves are closed, the response of the piping section is independent of the rest of the system. The response of the pipe section is driven by the value of the pipe section pressure at the instant that both valves attained the closed position. This pressure is the initial condition driving the homogeneous response. The homogeneous response is characterized by the relationship

$$\frac{p_2(t)}{R_L} = -\dot{m}(t) \tag{59}$$

or equivalently

$$
\begin{aligned}
0 &= \dot{p}_2(t) C_{EQ} + \frac{1}{R_L} p_2(t) \\
&= \dot{p}_2(t) + \frac{1}{R_L C_{EQ}} p_2(t)
\end{aligned}
\tag{60}
$$

The solution to equation (60) gives the isolated homogeneous pressure response of the pipe section:

$$
p_2(t) = p_2(0) \times e^{-t/(R_L C_{EQ})}
\tag{61}
$$

3.5 SIMULATION MODEL

The simulation models discussed are the non-dynamic propagation delay type and the lumped parameter type. These simulation models follow from the analytical models developed for the non-dynamic case, equations (16), (17) and (18) and for the lumped dynamic case, equations (48), (58) and (60). Contingent upon experimental model validation results, it may be necessary to extend these models to include spatially distributed parameters.

3.5.1 Non-Dynamic Propagation Delay Simulation Model

The simulation model for the non-dynamic case is shown in Figure 27. The model fluid supply is located on the left-hand side; the pressure from this fluid source is transmitted to the right through two piping sections. The piping sections may incorporate the propagation delay via a time delay element. End-valves and catastrophic pipe faults are modeled using a product element which essentially blocks the propagation of pressure to

the right. This simulation approach is characterized by unidirectional pressure propagation. Since the pressure propagation model employs time delays a direct interconnection of left and right unidirectional propagation models is feasible employing AND gate pressure logic combinatory, since the time delays would combine nonlinearly. Micro-controller action to regulate the end-valves is also incorporated into the simulation model. These consist of data storage and logical operator elements that sample the pressure in each piping section. The control logic configuration show will only allow a valve to remain open if pressure can be maintained by both of the pipe sections connected to the value. While suitable for the evaluation of some aspects of system performance, the model lacks the capability to directly integrate into an overall system simulation model which incorporates physical fluid phenomena directly. Due to this fact, an extension to dynamic modeling appears warranted.

3.5.2 Lumped Dynamic Simulation Model

Analytical lumped parameter models have been developed to describe the piping vessel pressure response to three operational cases. The first case corresponds to one end valve open and one end valve closed and is derived from equation (48) as

$$\frac{P_2(s)}{P_{1A}(s) \text{ or } P_{1B}(s)} = \frac{1}{\left(\dfrac{R_{EQ}}{R_L} + 1\right) + sC_{EQ}R_{EQ}} \tag{62}$$

The second case corresponds to the condition that exists when both end valves are open. This follows from equation (57) and is given by

$$\frac{P_2(s)}{P_{1A}(s) + P_{1B}(s)} = \frac{1}{\left(\dfrac{R_{EQ}}{R_L} + 2\right) + sC_{EQ}R_{EQ}} \tag{63}$$

The third and final case is the isolation response that results when both end-valves are closed. This follows from equation (59) as

$$0 = sP_2(s) + \frac{1}{R_L C_{EQ}} P_2(s) \tag{64}$$

Equations (62), (63) and (64) may be rearranged respectively into a common format suitable for generating a simulation diagram model with switched gains:

$$s\left(\frac{1}{\tau_{EQ}}\right)P_2(s) = P_2(s) - \left(\frac{R_{EQ}}{R_L} + 1\right)\left(P_{1A}(s) \text{ or } P_{1B}(s)\right) \tag{65}$$

$$s\left(\frac{1}{\tau_{EQ}}\right)P_2(s) = P_2(s) - \left(\frac{R_{EQ}}{R_L} + 2\right)\left(P_{1A}(s) + P_{1B}(s)\right) \tag{66}$$
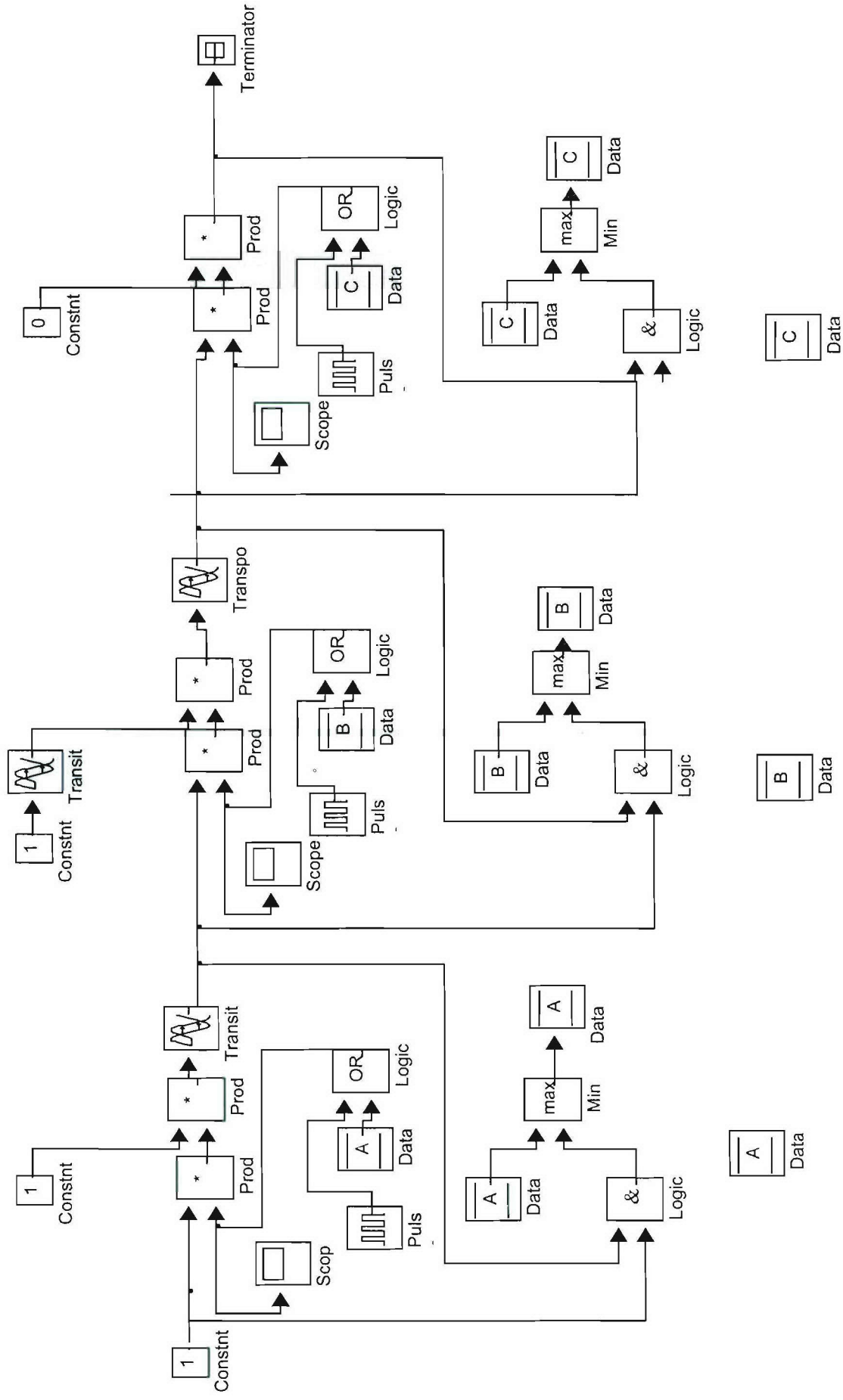
Figure 27: Non-dynamic simulation model diagram

$$s\left(\frac{1}{\tau_{EL}}\right)P_2(s) = P_2(s) \tag{67}$$

where

$$\tau_{EQ} = \frac{1}{C_{EQ}R_{EQ}} \tag{68}$$

and

$$\tau_{EL} = \frac{1}{C_{EQ}R_L} \tag{69}$$

The τ_{EQ} is the time constant associated with non-isolation, i.e. at least one of the piping section end-valves is open, while τ_{EL} characterizes the isolation case, i.e. when both of the end valves are closed.

Figure 30 shows the lumped parameter dynamic simulation model. This model represents a single piping section with end-valves. The simulation structure integrates the analytical models developed for the pipe section subject to only one end-valve open, both end-valves open and no end-valves open, i.e., isolation. The model is based on equations (66), (67), (68). These equations possess an identical simulation structure and the simulation model switches between them based on the system valve configurations: no, only one, or both end-valves open. The logic elements included decide which model is applicable based on end-valve control signals. In addition groups of this pipe/valve model segment are readily integrated into a complete UAV system model. This entails simply interconnecting the model segment pressure inputs to the pressure output of adjacent pipe

sections. Furthermore, any number of piping sections may be placed into a series-parallel topology.

An LP pipeline simulation model was constructed from the lumped dynamic sectional model previously presented. The pressure response behavior, which characterizes an LP air system, is illustrated in Figures 28 and 29. Figure 28 illustrates the charging of a 40 foot long pipe section to 100 psi with one end of the pipeline closed and the other end driven by a compressor. The pressure response along the pipeline is shown for a two second interval. In Figure 29, the LP air system begins charging as it did in Figure 28. At a time of one second the pipeline undergoes a rupture failure at a distance of twenty feet along the pipe with a cross sectional area large compared to the pipeline diameter. The pipeline is observed to discharge to ambient pressure on the closed end side and to go into a redistributed steady state flow on the supply side.
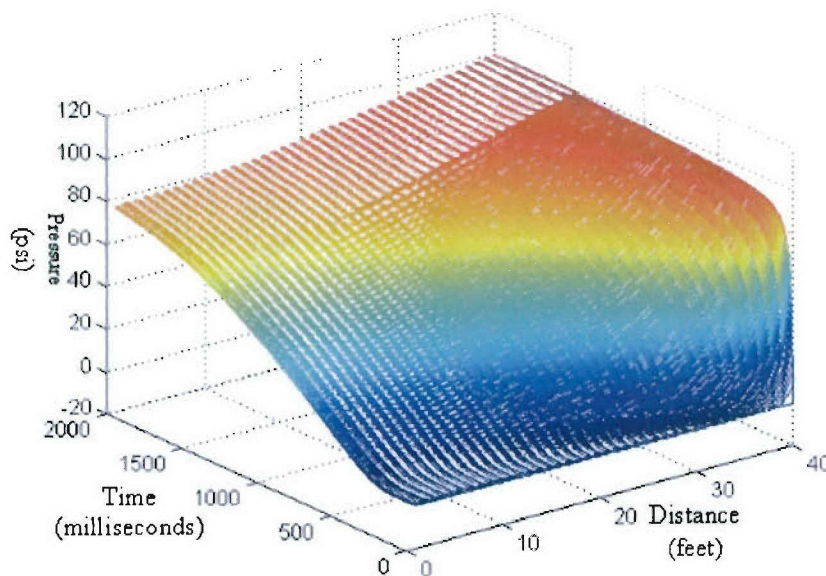
Figure 28: Simulation of distributed pressure profile along a charging LP air pipeline.
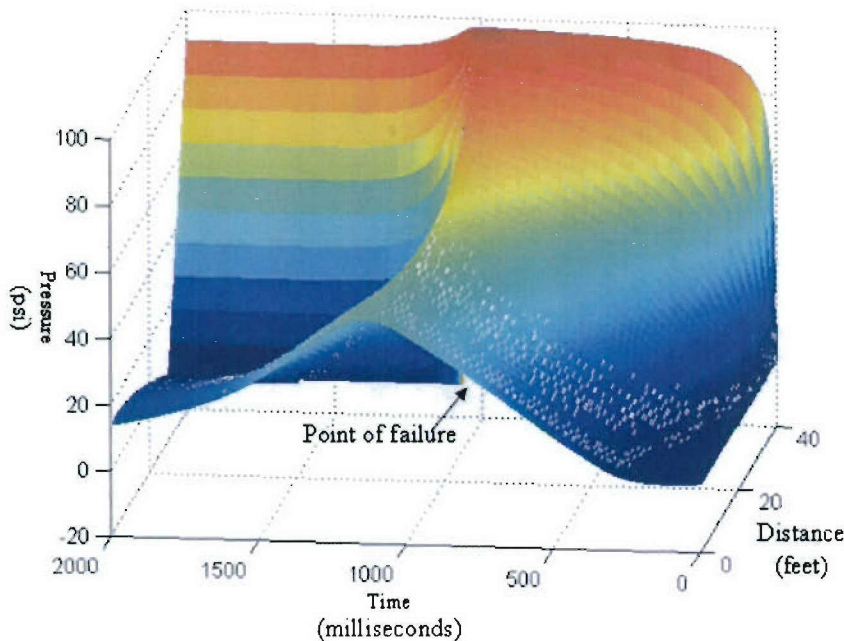
Figure 29: Simulation illustrating a charging LP pipeline that undergoes a catastrophic rupture failure located at distance 20ft. and occurring at time 1 sec.

3.5.3 Lumped Dynamic Leak Detection and Characterization

The process of leak detection and characterization must be accomplished with a set of pressure switch sensors. This sensor complement does not provide graduated pressure readings as may be employed in a response fitting algorithm such as least mean square or recursive least squares. Instead, the leak estimation problem must be solved in terms of the switching times of the pressure level switch sensors. These may be projected to yield an effective leakage decay time constant. The leakage decay time constant may be contrasted with the baseline non-leakage effective time constant. The magnitude of the deviation in the time constants yields an estimate of the severity of the leakage failure.
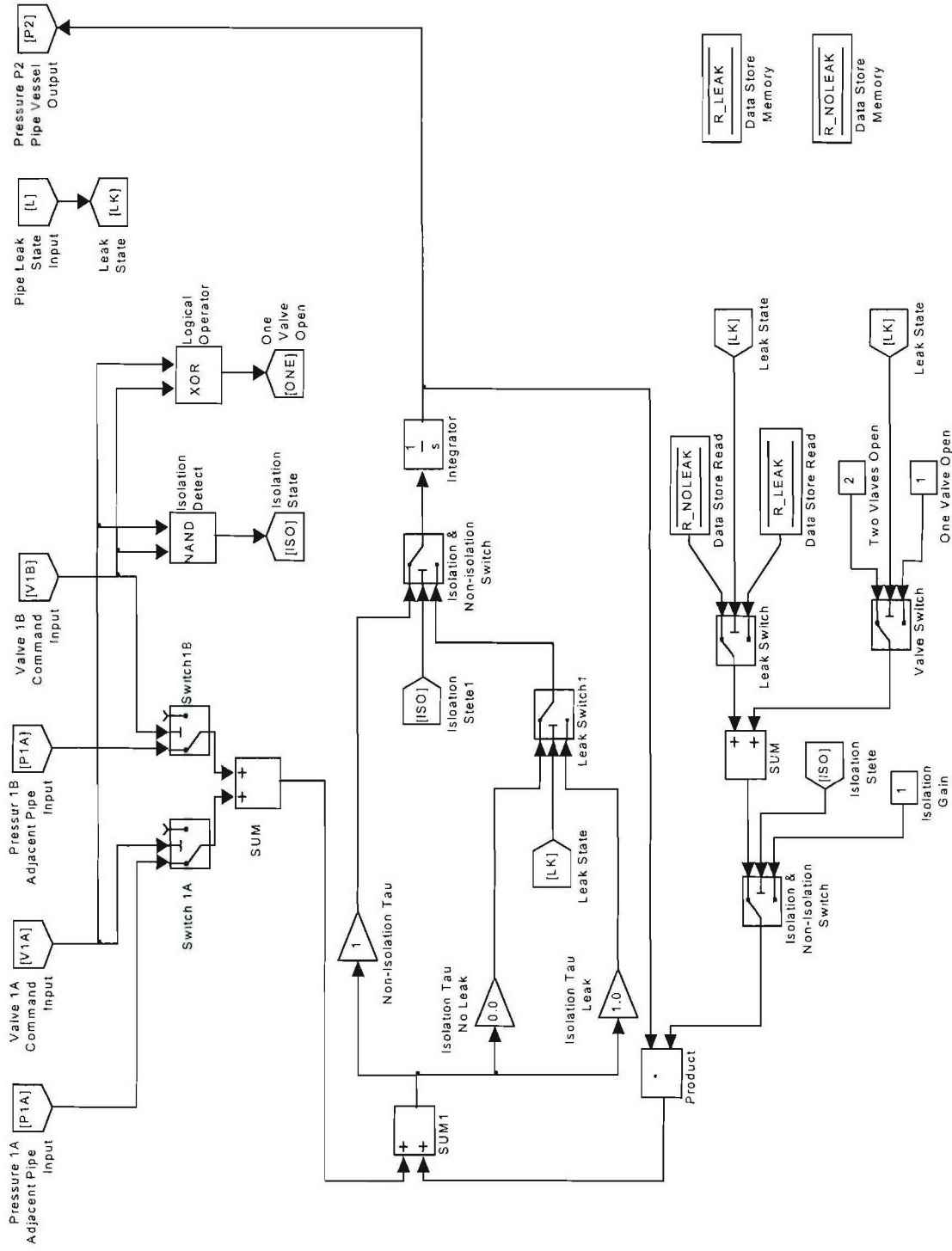
Figure 30: Lumped parameter dynamic simulation model.

3.6 Development Methodology for Autonomous Damage Mitigation

3.6.1 Implementation Approach

The fundamental problem of autonomous control development for distributed shipboard UAV systems is next addressed. An environmentally friendly and cost effective land-based UAV system was chosen as the initial development platform with results extending directly to other distributed shipboard systems, including potential hull structure damage assessment and control applications. A real-time simulation/emulation based methodology is introduced and employed to implement a prototype acoustic sensor array with the capability of detecting and locating acoustic sources within a distributed auxiliary supply system and has the potential to extend to more general and diverse distributed shipboard systems. The methodology is based on simulation/emulation and employs physically based modeling to characterize signals and the signal environment. The impetus for developing such a system is to devise a viable means of economically supplementing existing widely used pressure switch type sensors which are characterized by prohibitively long inertial lag responses precluding their use for dynamic fault detection and location. The use of non-supplemented switch type sensors requires quasi-steady switching to isolate faults and suffers from associated additional working fluid loss and the potential for extended algorithm convergence time. The prototype implementation employs simplified filtered threshold detection for event recognition and feature delay estimation. The filtering provides band limiting and along with environmental interference and noise reduction. The combination of reduced bandwidth coupled with simplified detection is aimed at reducing the computational and component

costs associated with higher bandwidth detection. Feature delay estimates are utilized in sensor-to-sensor feature propagation models to estimate the location coordinates of a fault source. Additionally, some aspects of implementing sensor nodes on other distributed shipboard systems and structures are considered.

3.6.2 Implementation Background

Aspects of dynamic modeling and switch sensor based autonomous damage control for UAV systems have been presented in [29], [10]. The general distributed architecture considered in these efforts has been adopted for the present application. A brief descriptive summary of the distributed architecture based on the above works provides a necessary perspective for the application.

The layout of a typical shipboard distributed fluid supply system configuration was shown in Figure 18. The system is comprised of an interconnection of series-parallel fluid flow piping paths with associated valves, sensors, micro-controllers and fluid supplies. The fluid supply units are compressors which feed the distributed system and are assumed to have relatively high volume baffle reservoirs. The flow control valve action is binary (e.g. on/off) and actuation is controlled by an associated micro-controller unit. The controllers each execute an independent algorithm whose action is based on two pressure switch sensors located on each side of the valve. Any of the piping sections and associated valves may experience a leakage failure. In this scenario, the operational goal is to autonomously mitigate damage impact by minimizing fluid loss and maximizing fluid supply to meet load demand.

A simulation model suitable for the analysis, design and implementation of autonomous control for switch sensor distributed fluid supply systems has been developed in [10]. The simulation is based on differential lumped modeling and incorporates the valve control actions of distributed micro controllers and leakage/blockage failure. The model predicts dynamic distributed UAV pipeline pressure and is based on simplified stagnation and flow equilibrium relations. The model is readily modified to incorporate other types of fluids and nonlinear flow pressure relationships. In addition, the model provides a basis for failure identification, condition assessment and autonomous damage control.

In the above UAV context, the present problem addresses the dynamic limitations of pressure switch sensors precluding response to system transitional dynamics which are precipitated by a sudden catastrophic damage failure in the piping and/or valves. This inability to sense rapid dynamics results in the loss information useful for the rapid location and assessment of system damage. However, the process of leak detection damage control can be accomplished with a set of pressure switch sensors as done by [30] using quasi-steady state sensing. A more detailed characterization of the nature of pressure switch sensor response follows.

### 3.6.2.1 Exiting Switch Sensor Characteristics

The pressure sensors associated with each piping valve detect whether the air pressure within the local section of pipe is above or below a reference threshold pressure range. The pressure sensor output is binary and provided by the opening and closing of a set of switch contacts. The pressure sensor input-output relationship between local pipe section

pressure and the sensor switch setting exhibits a hysteresis characteristic as illustrated in Figure 31. The sensor threshold pressure is defined to be

$$T_{SR} \equiv \frac{T_{SL} + T_{SH}}{2} \tag{70}$$
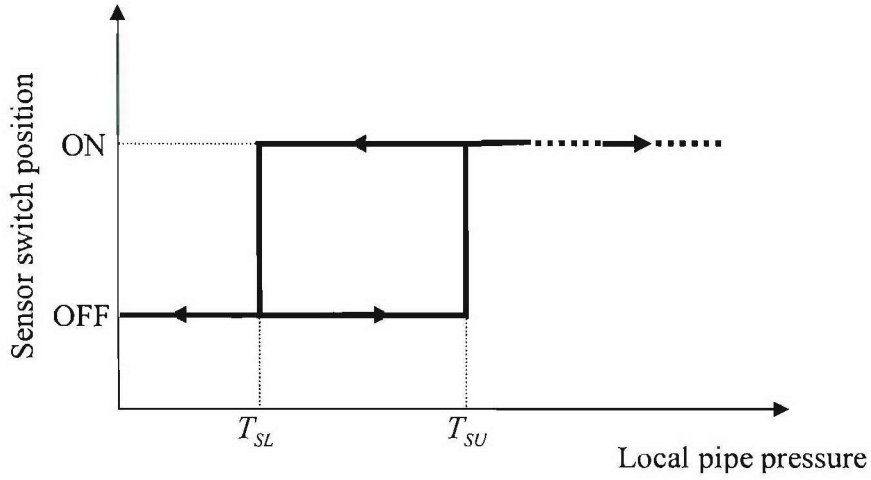
Figure 31: Pressure sensor switch response as a function of quasi-steady state local pipe pressure.

The conservation of mass is applicable to both dynamic and steady state responses and, for fluid velocity v and fluid density ρ, may be expressed as

$$\frac{\partial \rho}{\partial t} = -\frac{\partial (v\rho)}{\partial t} \tag{71}$$

and in the case of incompressible flow the fluid density is constant yielding

70

$$0 = \frac{\partial \rho}{\partial t} = -\frac{\partial(v\rho)}{\partial t} \qquad (72)$$

with the consequence that velocity of the fluid is constant with respect to position. This requires that the system remain in steady state thus not exhibiting any unsteady behavior. The application of time varying forcing flow and pressure generate a quasi-steady state response. In the case of a compressible fluid the inertial lag in pressure switch sensor dynamics results in a complete lack of response to and sensing of the time varying wave dynamics of (71) and quasi-steady state forcing dynamics of (72).

3.6.2.3 Fluid Flow Characterization

The relations for motion, continuity and momentum are employed to characterize the compressible fluid flow within the UAV system. In the case of unsteady state fluid flow, the unsteady flow occurs when the fluid motion at any point along the system is a function of time. Initial assumptions about the fluid flow are that it is isentropic and one-dimensional. An isentropic flow is both adiabatic, i.e. one in which no heat is transferred to or from the fluid, and reversible neglecting friction and other effects. The assumption of one-dimensional flow neglects variations in fluid velocity and pressure transverse to the primary flow direction.

Given the inability of switch sensors to sense unsteady flow, the location of leak damage must be determined by steady state switching of fluid through the system resulting in added fluid loss and potentially extended convergence time of the switching algorithm. If the fluid pressure dynamics could be sensed by switch sensors, the leak estimation problem could be solved more rapidly in terms of the dynamic switching times

of the pressure level switch sensors. These may be projected to yield an effective leakage decay time constant. The leakage decay time constant may be contrasted with the baseline non-leakage effective time constant. The magnitude of the deviation in the time constants yields an estimate of the severity and location of the leakage failure.

The above transient dynamic approach to leak detection necessitates the implementation of dual wide bandwidth pressure sensors at each valve location with associated increases in cost and processing overhead. In contrast, the approach taken here is to supplement the existing pressure switch sensor with inexpensive low bandwidth, i.e. low processing overhead, acoustic sensors. The easily mounted supplemental sensors can be used to generate impact damage location estimates based upon impact and valve switching acoustic dynamics. This approach relies on the application of source localization techniques subject to the constraints imposed on vibration propagation in the shipboard distributed system under consideration.

3.6.3 TRANSDUCER CONDITIONING

The analysis of the characteristics of actual sampled acoustic signals reveals the nature of the signal environment and the requirements of conditioning to in attempting to optimize acoustic source location algorithm performance. In addition the conditioning function may serve in the capacity of an anti-aliasing filter.

3.6.3.1 Signal Environment

A characteristic sampled acoustic signal within the distributed deployment environment is shown in Figure 32. The signal environment was found to have a high degree of power
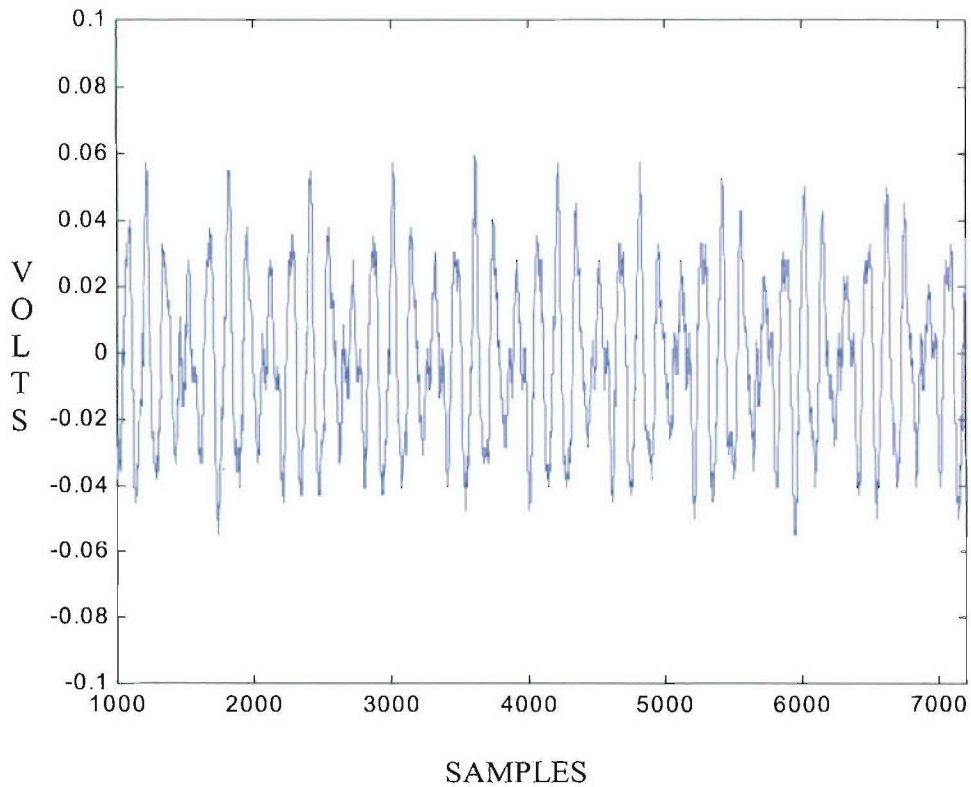
Figure 32: Unconditioned acoustic sampled acoustic signal

line interference. The source signal is quasi-periodic with some nonlinear distortion introduced by the acoustic transducer generating the signal. The interference beat pattern generated by the source signal and power line components is also observable. It was observed that the power line frequency and associated harmonics exhibited a presence up to a bandwidth of approximately 300 Hz. Various processing approaches were evaluated to mitigate the impact of power line frequency interference. These methods employed numerical passband filtering, nulling, autocorrelation and cross-correlation. This approach was found to have a prohibitive turn around time due to the computational complexity inherent in these methods. Consequently, a conditioning circuit was employed.

The adjusted frequency response of the conditioning circuit is shown in Figure 33.
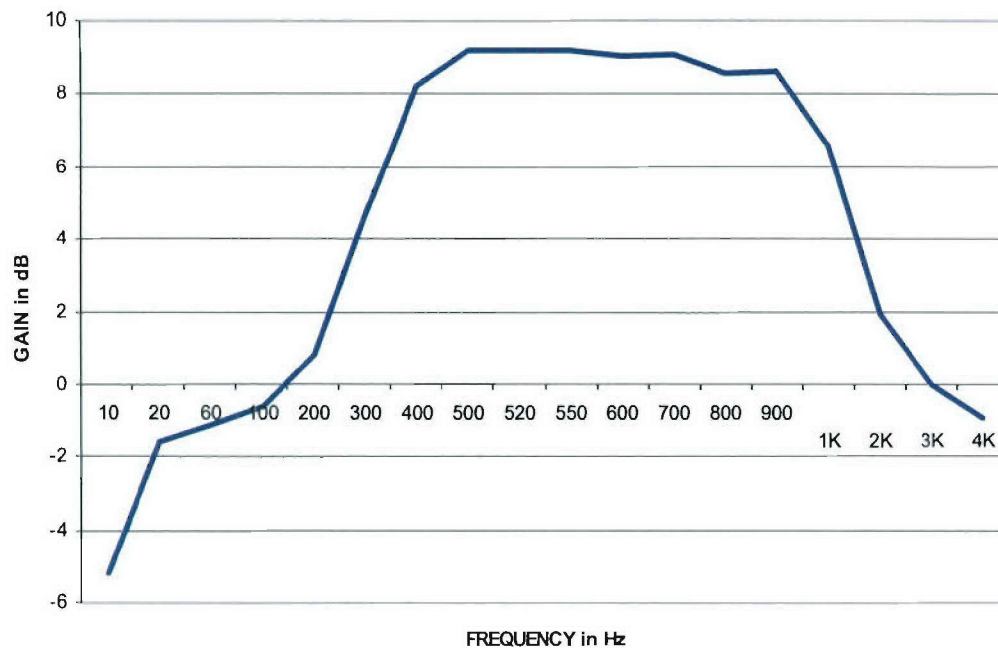
Figure 33: Adjusted measured frequency response of conditioning

This response compensates for the acoustic element producing a net flat passband characteristic. The lower cutoff frequency must be chosen to assure that power line primary and harmonic frequencies are sufficiently suppressed. The upper cutoff frequency serves the dual function of reducing interference from higher frequency sources and also providing anti-aliasing filtering for the sampling process while assuring sufficient spatial sampling to resolve the source position information.

3.6.3.2 PROTOTYPE

The prototype employs threshold detection to determine the presence of sources and to estimate feature propagation delay amongst the acoustic sensor configuration. The fusion of the sensor-to-sensor feature delay lends itself to a graphical representation which could be utilized to generate a graphic display showing the deployment environment and estimated source location.

#### 3.6.3.2.1 Detection and estimation

Characteristic sample signals of an acoustic burst within the deployment environment are shown in Figure 34. The signals constitute a signal power and noise power within the bandwidth of the system. The objective is to perform source detection and localization capable of operating at minimal signal to noise ratio (SNR). Assuming a Gaussian white noise process, the optimum processing approach may be extrapolated for correlation and square-law based detection and estimation as [9] and [20].

The propagation delay of acoustic signals is core to estimating the location of sources. The propagation velocity of sound is a function of temperature and material, e.g. for air the propagation velocity may be expressed as

$$V_{sound} = 1088\sqrt{1 + \frac{^{\circ}C}{273}} \quad fps \tag{73}$$

If the signal sources are from a set of characterized signal sources, the optimum processing system may be based on cross correlation. The correlation process compares a reference signal, $r(t)$, with the sampled signal, $s(t)$, employing the cross correlation

$$C_{sr} = \int_{t_1}^{t_2} s(t)r(t+T)dt \tag{74}$$
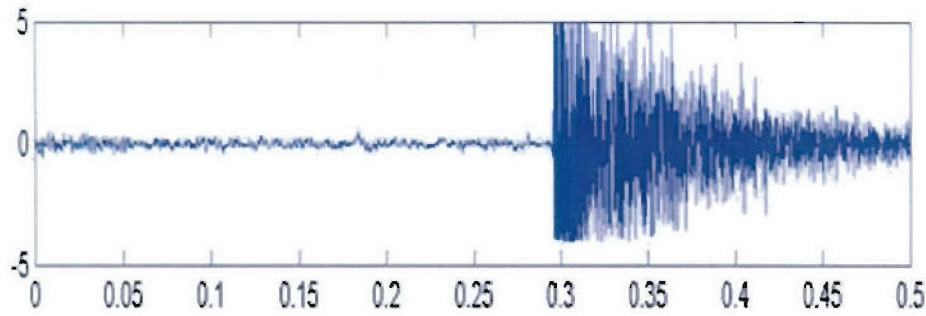
Figure 34: Characteristic acoustic burst sample

The cross correlation will be a maximum when T represents the physical time delay due to propagation of the acoustic wave. The computational effort associated with the cross correlation function may be prohibitive in achieving real-time sampling and detection turn around time in implementation.

If the characteristics of the acoustic source are unknown or the computation associated with the cross correlation function is of prohibitive complexity, square law based detection and estimation may be a viable alternative. The processing of a signal occurs over a time interval τ and over a bandwidth w. The output of the processing may be the time average of the detected signal voltage or power (i.e. square law based processing). For the interval τ, a decision must be made as to whether an acoustic signal is present. This is accomplished by setting a threshold level for the output of the processing function over the processing time interval. It is desired to have the processing time interval as short as possible for real-time implementation feasibility. The detection and performance thresholds for the cross correlation and square law threshold based approaches are given by [9] and [20].

76

$$D_{cross\ correlation} = 10\log\{SNR\} \tag{75}$$

and

$$D_{square\ law} = 5\log\{SNR\} \tag{76}$$

Square law based detection and estimation was implemented in the prototype since the acoustic sources are not characterized sufficiently for cross correlation computation and also to avoid the computational complexity of cross correlation in real-time implementation. In the prototype case, the square law process is approximated by absolute magnitude possessing with respect to a threshold. The fundamental problem is to trade off as little performance as possible in transitioning from correlation-based detection and estimation to that of square law based processes.

3.6.3.2.2 DOA/TDOA Localization

The hyper-geometric characterization of source location with respect to a constellation of sensors is illustrated in Figure 35 without loss of generality, the source is located at coordinates (8,10) while the sensors are symmetrically located at (0,-5) and (0,5) respectively without loss of generality. The source is in a near field configuration, approaching the asymptotic region, with respect to the sensors [9], [4]. The resulting DOA estimate for this configuration is depicted as a straight line plot emanating from the origin. The intersection of this plot with the hyper-geometric curve represents an estimate of the source location. The appropriate hyperbolic curve is selected based on the time of arrival of the acoustic wave at the various sensors. In the case illustrated, the signal arrives at Sensor 1 first indicating that the right-side of the hyperbolic curve contains the

source. Due to the geometric symmetry, an alias source is present at coordinates (8,-10). The correct source location must be determined by corroborating TDOA location data from other sensor platforms.

The hyper-geometric curves are characterized by the relation

$$\frac{x^2}{a^2} - \frac{y^2}{c^2 - a^2} = 1 \tag{77}$$

where $\pm c$ are the sensor locations, i.e. foci, and $\pm a$ are the vertices of the hyperbola and represent the intersection points of the hyperbola with the transverse axis. If t_{12} is the waveform time delay from sensor 1 to sensor 2, then

$$a = \frac{v t_{12}}{2} \tag{78}$$

where v is the velocity of wave propagation. If three or more sensors are present then, given the relative time delays associated with each sensor pair, the source location may be uniquely selected from the intersection of two hyperbolic curves given by

$$x^2 = \frac{\left(b_x^2 + a_y^2\right)}{\left(\dfrac{b_x^2}{a_x^2} - \dfrac{a_y^2}{b_y^2}\right)} \tag{79}$$

$$y^2 = \frac{\left(b_y^2 + a_x^2\right)}{\left(\dfrac{b_y^2}{a_y^2} - \dfrac{a_x^2}{b_x^2}\right)} \tag{80}$$

The above approach to source location employs a blend of DOA and TDOA methods. The method produces conjugate aliased source location estimates. Two source regions have been provisionally recognized: (1) a near field region exhibiting reduced sensitivity and higher resolution; (2) an asymptotic region (far-field) exhibiting greater sensitivity and reduced resolution. The source location data produced is appropriate for transmission in a UAV communications network for corroboration to remove conjugate alias source locations.
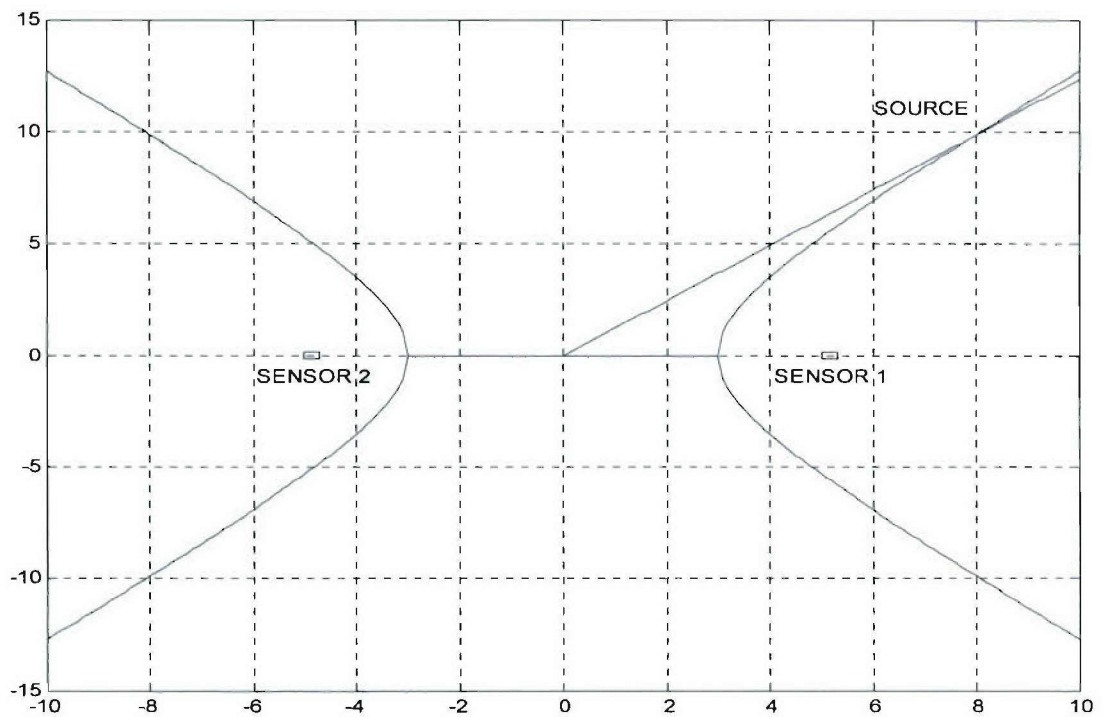
Figure 35: Illustration of the combined localization approach.

4.0 APPENDIX A: Matlab Shell Code

Matlab/Mfile for navigation around a circular obstacle

```
clear
simin=[0,0]
simin1=[0,0]
simin2=[0,2]
simin3=[0,2]
path1=simin2(2)
path2=simin3(2)
t(1)=0

for i=1:1:40

  sim('circ3')
  [r,c]=size(simout)
  [r1,c1]=size(simout1)
  [r3,c3]=size(simout3)
  [r2,c2]=size(simout2)
  [rt,ct]=size(tout)
  path1(i+1)=simout2(r2)
  path2(i+1)=simout3(r3)
  t(i+1)=t(i)+tout(rt)
  simin=[0,simout(r)]
  simin1=[0,simout1(r1)]
  simin2=[0,simout2(r2)]
  simin3=[0,simout3(r3)]

  plot(path1,path2,'-*')
   center=[4 4]
radius=[.58]
NOP=[1000]

THETA=linspace(0,2*pi,NOP);
RHO=ones(1,NOP)*radius;
[X,Y] = pol2cart(THETA,RHO);
X=X+center(1);
Y=Y+center(2);
H=plot(X,Y,'r');
axis square;
 hold on
 axis([-1,11,-1,11])


 grid
end
```

4.1 APPENDIX B : Overview of Fuzzy Fusion Methodology

INFORMATION: QUANTITY/DIVERSITY

Integration Challenge:

- Complexity common in a *single system*
- Compounded at the *platform level*

Heuristically:

- Some mechanism is needed to fuse diverse data and extract information

A *fuzzy* based mechanism chosen:

- Natural language base
- Linguistically based if-then rules allow "apples and oranges"
- Flexible rule add/remove/change (associative evaluation)
- Incorporates experience of experts in rule base
- Work in concert with existing control techniques

A COMBINATION OF MODEL-BASED AND FUZZY INFERENCE APPROACHES

Model-based body:

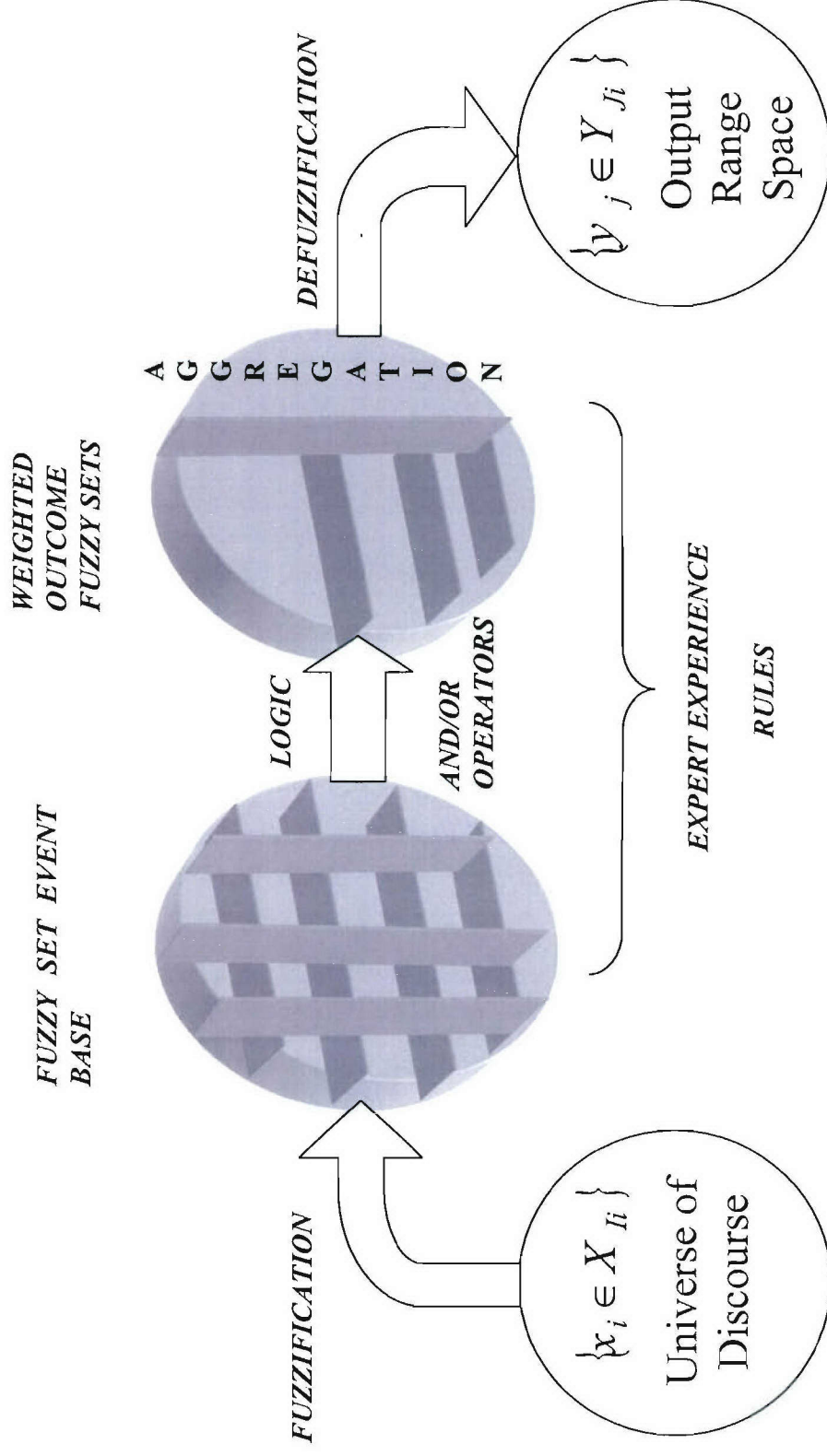- *Existence* of models
- Derived from and embody the *physics* of the plant
- Provides a framework for *interpretation* of behavior and *condition assessment*
- Many controller *design approaches* are model based

Fuzzy inference intelligence:

- *Flexible* linguistic rule structure
- Driven by *deviations* in measurements and model estimates
- *Fusion and decision* mechanism

FUZZY PROCESS MAPPING

FUZZY INFERENCE PROCESS

Crisp Inputs	Fuzzification	Antecedent	Consequent	Aggregation	Defuzzified Crisp Output

MEASUREMENTS

CLASSIFICATION OF EVENTS

GROUP OF EVENT SETS

WEIGHTS CONCLUSIONS

CONCLUSIONS COMBINED

CONVOLUTION REGARDS
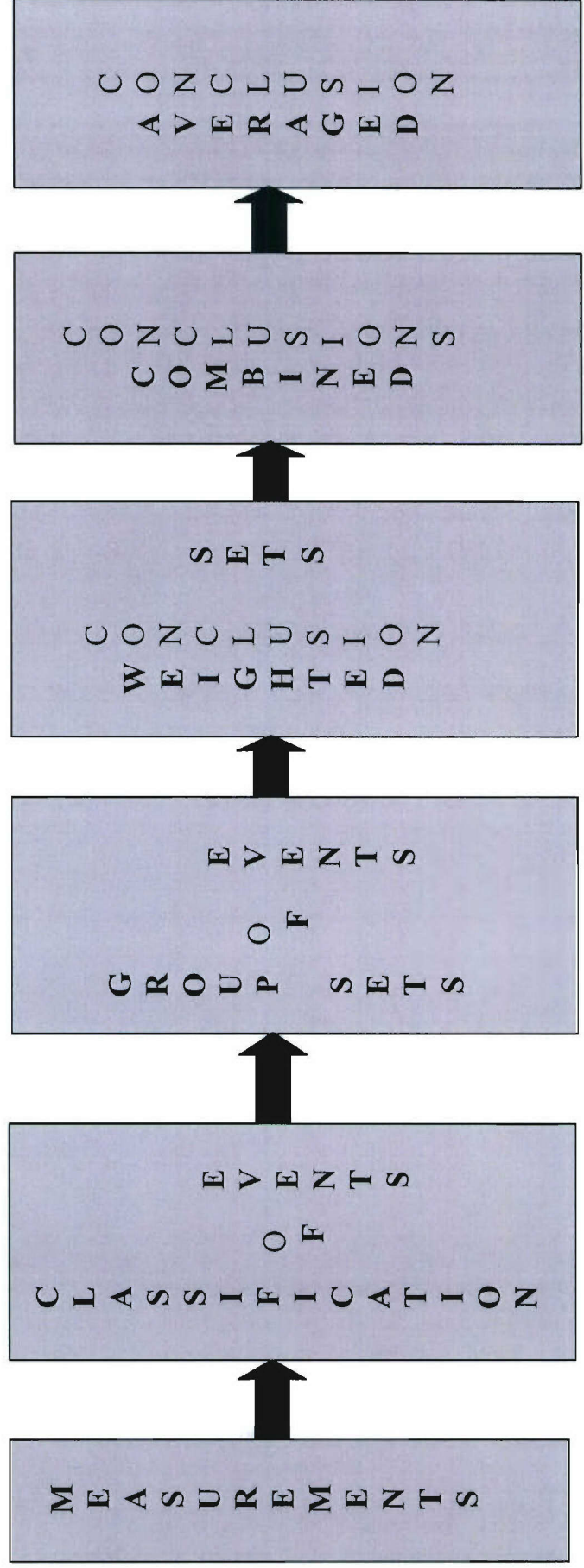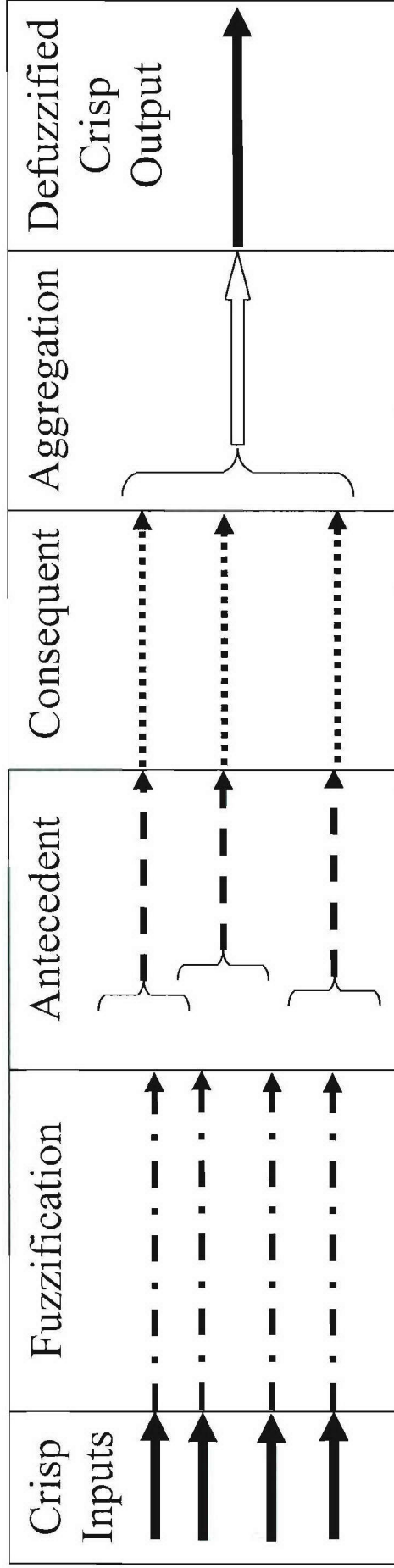
CRISP INPUTS

State Deviation Vector Elements:

$$x_{\Delta i}(t) = \left\| \frac{x_{Pi}(t) - x_{Mi}(t)}{x_{Mi}(t)} \right\|$$

Output Deviation Vector elements:

$$y_{\Delta i}(t) = \left\| \frac{y_{Pi}(t) - y_{Mi}(t)}{y_{Mi}(t)} \right\|$$

FUZZIFICATION
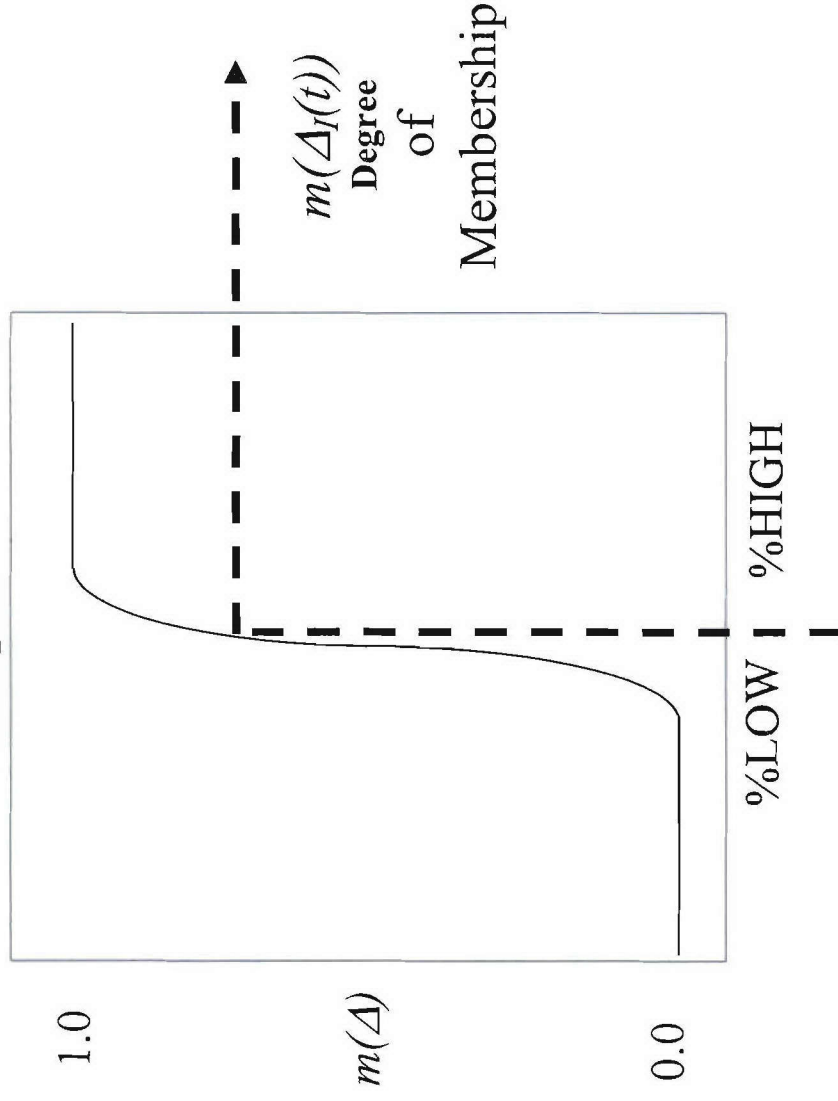
Extension of Classical
"Crisp" Set Theory

FUZZY SET
A_I
Significant error event

FUZZY ELEMENT
$(\Delta_I(t), m(\Delta_I(t)) \; ? \subset ? \; A_i$

Membership Function

$m(\Delta_I(t))$
Degree
of
Membership

1.0

$m(\Delta)$

0.0

%LOW   %HIGH
%

INPUT
$\Delta_I(t) = y_{\Delta i}(t) \; or \; x_{\Delta i}(t)$

LINGUISTIC RULE

If $\underline{(A_1 \text{ and/or } A_2 \ldots \text{ and/or } A_N)}$ then $\underline{(Z)}$

If $\underline{v_{Ai}(t)}$ small and only one $x_{Ai}(t)$ large   then   confidence level is high

Antecedent

Consequent

- Assigned a *degree of membership* based on fuzzified inputs:

$$(\Delta_I(t), m(\Delta_I(t)) \, ? \subset ? \, A_I$$

- Logical operations:
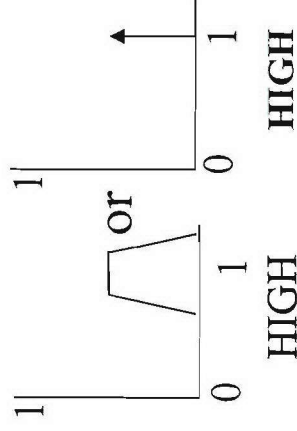
$$OR \equiv max(m(\Delta_I(t), m(\Delta_J(t))$$

$$AND \equiv min(m(\Delta_I(t), m(\Delta_J(t))$$

- Result is a *single number* from *0 to 1.0* representing the degree to which the antecedent event has occurred

- One *distributed* or *crisp singleton* membership function outcome:

LOW   MED   HIGH   HIGH

Confidence Level Membership Functions

- Weighted outcome:

HIGH   HIGH
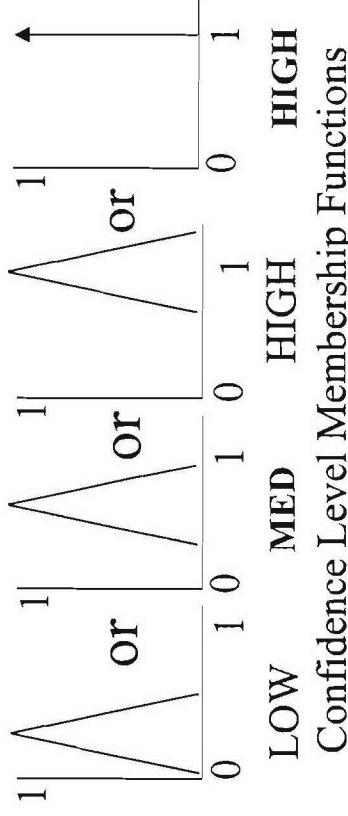
AGGREGATION

Apply the OR operator to:

- *combine the individual weighted* rule outputs to a single fuzzy or crisp set
- this represents the *overall* outcome

For example letting OR ≡ max generates the aggregate membership function:

$\mu(x^1)$

or

$\mu(x^1)$
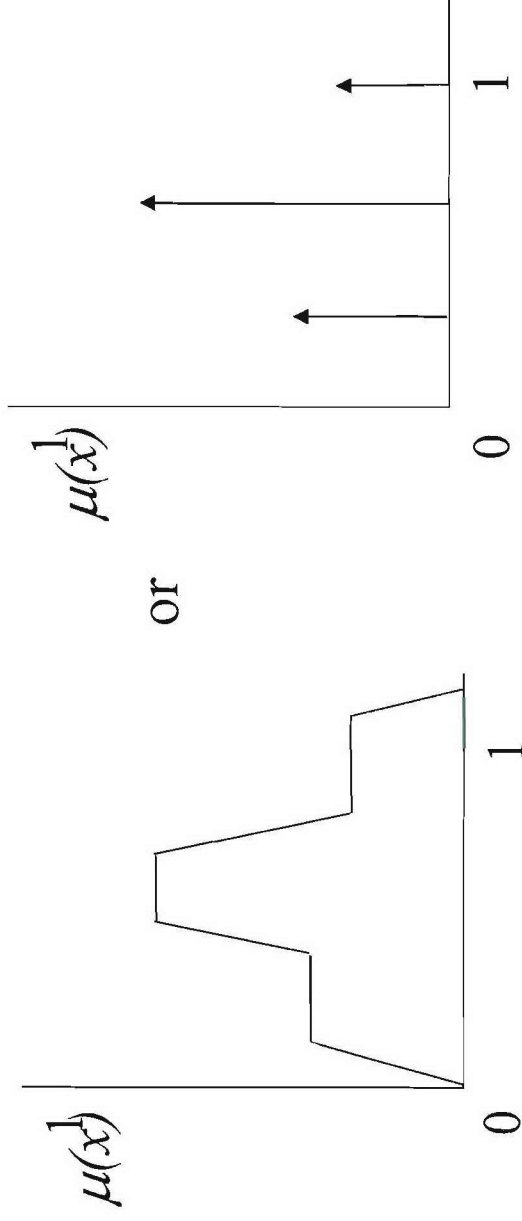
DEFUZZIFICATION

Defuzzification:

- start with the *aggregate fuzzy set*
- generate a *single number* output
- the output represents the *fusion* of all conditions

Centroid approach:

$$\bar{x} = \frac{\int \mu(x)zdz}{\int \mu(x)dx}$$

Singleton case: $\bar{x} = \dfrac{\sum_i \delta_i(z - z_i)z_i}{\sum_i \delta_i(z - z_i)}$

5.0 REFERENCES

[1] Binder, R. C., *Fluid Mechanics*, Englewood Cliffs, NJ, Prentice-Hall, 1958.

[2] Borrie, J. A., *Modern Control Systems - A Manual of Design Methods*, Prentice-Hall, NY, 1986.

[3] Bullock, D. and Grossberg, S., "Neural Dynamics of Planned Arm Movements: Emergent Invariants and Speed-Accuracy During Trajectory Formation", *Psychological Review*, Vol. 95, No. 1, 1988.

[4] Chen, J. C., Hudson, R. E., and Yao, K., "Maximum likelihood source localization and unknown sensor location estimation for wideband signals in the near-field," *IEEE Transactions on Signal Processing*, pp. 1843-1854, August 2002.

[5] Clark, V., "Projecting Decisive Joint Capabilities", *Proceedings of the United States Naval Institute*, October 2005.

[6] D'Azzo, J. J., and Houpis, C. H., *Linear Control System Analysis and Design,* third edition, McGraw-Hill, NY, 1988.

[7] Gerhart, P. M., Gross, R. J. and Hochstein, J. I., *Fundamentals of Fluid Mechanics*, second edition, Reading, MA, Addison Wesley, 1992.

[8] Haykin, S., *Adaptive Signal* Processing, Prentice-Hall, Englewood Cliffs, NJ, 1996.

[9] Kinsler, L., et. al., *Fundamentals of Acoustics*, 3rd edition, Wiley, NY, 1982.

[10] Konyk, Jr., S. and M. Kusewski, "Autonomous Control Architecture Model Development for Shipboard Fluid Supply Systems", *Intelligent Ship Symposium IV*, April 2001.

[11] Konyk, Jr., S., and Jin, Y.,"Spatial Array Filtering Employing a Nonlinear Constraint Measure", *Proceedings of the 1997 IEEE National Radar Conference*, May 1997.

[12] Konyk, Jr., S., and Tolotta, V., "Dynamic Modeling and Control of a Gas Turbine Engine" *Proceedings of the ASNE Intelligent Ships Symposium II,* Philadelphia, PA, November 1996.

[13] Konyk, Jr., S. and Tolotta, V., "A Fuzzy Framework for the Operational Control of a Gas Turbine Propulsion Engine", *Proceedings of the American Society of Naval Engineers Intelligent Ships Symposium III*, Philadelphia, PA, June 1999.

[14] Konyk, Jr., S.,"Manipulator Control with Inherent Neuro-Physiologically Derived Motion Constraints and Learning", *Proceedings of the 1993 International Conference on Intelligent Autonomous Systems (IAS-3)*, Pittsburgh, PA, February, 1993.

[15] Konyk, Jr., S. "Dynamic Trajectory Evolution Incorporating Modeling of Arm Movement Neural Data", *Proceedings of the 1992 IEEE International Conference on Intelligent Robots and Systems (IEEE IROS'92)*, Raleigh, NC, July, 1992.

[16] Konyk, Jr., S., Amin, M. G. and Lagunas, M. G., "Null Subspace Framework for Nonlinearly Constrained Solutions", *Proceedings of the European Signal Processing Conference (EUSIPCO 90)*, Barcelona, Spain, 1990.

[17] Konyk, S., Jr. and W. D. Cheung, "Neuromorphic path generation in real-time", *Proceedings of the 15th Annual Conference of the IEEE Industrial Electronics Society*, Philadelphia, PA Nov., 1989.

[18] Konky, S., Jr., Metzer, J. and Swaminathan, A., "Distributed Automata Techniques for Surface Platform Autonomous Control and Survivability in Naval Applications", *Intelligent Ships Symposium VI*,2005.

[19] Konyk, S., Jr., M. M. Zerby and M. L. Kuszewski, "Development of Self-Actuating Distributed Auxiliary System Control and Sensing for Damage Mitigation", with M. M. Zerby and M. L. Kuszewski, *Proceedings of the American Society of Naval Engineers Intelligent Ships Symposium V*, with Michael Kuszewski, Philadelphia, PA, May 2003.

[20] Mahajan, A. and Walworth, M., "3-D position sensing using the differences in the time-of-flights from a wave source to various receivers," *IEEE Transactions on Robotics and Automation*, pp. 91-94, February 2001.

[21] Maybeck, P., *Stochastic Models, Estimation and Control,* vol. 1, Academic Press, NY, 1979.

[22] Nauck, D., Klawonn, F., and Kruse, R., *Foundations of Neuro-Fuzzy Systems,* John Wiley & Sons, NY, 1997.

[23] Potter, M. C., *Fundamentals of Engineering*, Great Lakes Press, Okemos, MI, 1999.

[24] Passino, K. M., and Yurkovich, S., *Fuzzy Control*, Addison Wesley, NY, 1998.

[25] Ross, T. J., *Fuzzy Logic with Engineering Applications*, McGraw-Hill, NY, 1995.

[26] Sears, F. W., Zemansky, M. W. and Young, H.D. *University Physics*, sixth edition, Reading, MA, Addison Wesley, 1982.

[27] Tchangov, T., and Konyk, Jr., S., "Implementation Aspects of MEMS Sensor Array for Sound Target Localization", with T. Tchangov, *Proceedings of the International Conference on Automatics and Informatics*, Sophia, Bulgaria, May 2001.

[28] Tufts, D., and Kumaresan, R., "Estimation of frequencies of multiple sinusoids making linear prediction perform like maximum likelihood," *Proceedings of the IEEE*, pp. 975-989, 1982.

[29] Widrow, B., and Stearns, S., *Adaptive Signal Processing*, Prentice-Hall, Englewood Cliffs, NJ, 1985.

[30] Zerby, M. and Rogers, J., "Control Scheme for Damage Reconfiguration of a Compressible Fluid System Using Distributed Control Without Network Communications", *Intelligent Ships Symposium IV*, April 2001.

[31] Zurada, J. M., *Introduction to Artificial Neural Systems*, West Publishing Company, NY, 1992.

REPORT DOCUMENTATION PAGE

The public reporting burden for this collection of information is estimated to average 1 hour per response, including the time for reviewing instructions, searching existing data sources, gathering and maintaining the data needed, and completing and reviewing the collection of information. Send comments regarding this burden estimate or any other aspect of this collection of information, including suggestions for reducing the burden, to Department of Defense, Washington Headquarters Services, Directorate for Information Operations and Reports (0704-0188), 1215 Jefferson Davis Highway, Suite 1204, Arlington, VA 22202-4302. Respondents should be aware that notwithstanding any other provision of law, no person shall be subject to any penalty for failing to comply with a collection of information if it does not display a currently valid OMB control number. **PLEASE DO NOT RETURN YOUR FORM TO THE ABOVE ADDRESS.**

1. REPORT DATE (DD-MM-YYYY)	2. REPORT TYPE	3. DATES COVERED (From - To)
December 2005	Final	31 June 2004 - 1 September 2005

4. TITLE AND SUBTITLE

Distributed Autonomous Control Action Based on Sensor and Mission Fusion

5a. CONTRACT NUMBER

5b. GRANT NUMBER

N00014-04-1-0620

5c. PROGRAM ELEMENT NUMBER

6. AUTHOR(S)

Stephen Konyk, Jr. (PI)

5d. PROJECT NUMBER

5e. TASK NUMBER

5f. WORK UNIT NUMBER

7. PERFORMING ORGANIZATION NAME(S) AND ADDRESS(ES)

Villanova University - Center for Advanced Communications
800 Lancaster Avenue
Villanova, PA 19085

8. PERFORMING ORGANIZATION REPORT NUMBER

5-27728

9. SPONSORING/MONITORING AGENCY NAME(S) AND ADDRESS(ES)

Office of Naval Research
Code 313
875 N. Randolph Street
One Liberty Center
Arlington, VA 22203-1995

10. SPONSOR/MONITOR'S ACRONYM(S)

ONR

11. SPONSOR/MONITOR'S REPORT NUMBER(S)

12. DISTRIBUTION/AVAILABILITY STATEMENT

Approved for Public Release; Distribution is Unlimited

13. SUPPLEMENTARY NOTES

14. ABSTRACT

The proposed research effort focuses on the exploration of sensing and control techniques in the framework of fusion and distributed control pertinent to the problem of deploying autonomous unmanned surface platforms and clusters of platforms in mission applications in support of future naval capability. The considerations which comprise the approach to the distributed autonomous problem are threefold: (1) platform sensing capability for environment and mission; (2) distributed based control of autonomous platforms and clusters; (3) the intelligent fusion of sensor data, mission and control action. Fundamentally, the effort deals with the study of pertinent modeling approaches which may be useful in enhancing the processing and fusion of data to achieve appropriate distributed control action. This provides a vehicle for the exploration of mission specific distributed autonomous platform performance. From an application perspective, the real-time turnaround, detection correlation and adaptability of a fusion based distributed control are of concern. These concerns require the development of approaches to sensor and mission fusion.

15. SUBJECT TERMS

Unmanned Autonomous Vehicles; Autonomous Navigation; Shipboard Auxiliary Systems; LP Air; Damage Control; Automation

16. SECURITY CLASSIFICATION OF:			17. LIMITATION OF ABSTRACT	18. NUMBER OF PAGES	19a. NAME OF RESPONSIBLE PERSON
a. REPORT	b. ABSTRACT	c. THIS PAGE			Stephen Konyk, Jr.
U	U	U	UU	100	19b. TELEPHONE NUMBER (Include area code) 610-519-4983